accepted for publication in "International Journal of River Basin Management" (May 2025)

Numerical Modelling of Navigable Waterways using a Discontinuous Galerkin Method: Study of Meuse River – Campine Canal flow

Amit Ravindra Patil [a,b]*, Fabricio Fiengo Perez[c], Jonathan Lambrechts[b], Insaf Draoui[b], Eric Deleersnijder[b,d] and Benjamin Dewals[e]

[a] *Belgian Nuclear Research Centre, Mol, Belgium.*

[b] *Institute of Mechanics, Material and Civil Engineering, Université catholique de Louvain, Louvain-la-Neuve, Belgium*

[c] *Aquafin, Aartselaar, Belgium*

[d] *Earth and Life Institute, Université catholique de Louvain, Louvain-la-Neuve, Belgium*

[e] *Research unit Urban & Environmental Engineering (UEE), Hydraulics in Environmental and Civil Engineering (HECE), University of Liege, Liege, Belgium*

*Corresponding author: Amit Ravindra Patil; amitravindra.patil@sckcen.be

Numerical Modelling of Navigable Waterways using a Discontinuous Galerkin Method: Study of Meuse River – Campine Canal flow

Flow in navigable rivers is generally controlled by hydraulic structures, such as weirs. The numerical representation of such structures requires special consideration. In this study, we introduce a new numerical technique to represent these structures in a discontinuous Galerkin method. Compared to other methods, the new approach offers more flexibility in terms of node treatment and better stability by reducing sensitivity to flux treatment. The model is demonstrated on a real case study, the Meuse River and its canal network in Belgium. The simulation outcomes are in good agreement with the available measurements. The inclusion of the operational rules of the hydraulic structures in the model allowed the representation of the flow in a large navigation system (about 450 km of river and canal network) and the simulation of the discharge distribution for a wide range of flow regimes in the Meuse River and the associated canals. The DG method proved capable of handling different hydraulic structures, such as weirs and sluice gates, within complex flow networks. Finally, the influence of alternative implementations of the weir operation rules on the computed discharge in the Meuse River is evaluated.

Keywords: Hydraulic structures; river-canal systems; modelling; Discontinuous Galerkin method; Meuse River.

1. Introduction

Hydraulic structures, such as weirs, are widely used to allow navigability in waterways, flood control, irrigation, and numerous other purposes. Nowadays, most shallow water models are capable of simulating water flow in river systems by taking into account the influence of these hydraulic structures. However, the implementation of such structures in shallow water models requires specific considerations that depend on the type of numerical method. Hydraulic structures introduce discontinuities in the water surface profile and, in the near-field of the structures, pressure distribution is not hydrostatic (García-Alén *et al*. 2021, Zerihun and Fenton 2007). Existing shallow-water models incorporating hydraulic structures typically fall into one of the following categories, depending on the method employed for integration of the equations: (1) finite differences (FDM), (2) finite volumes (FVM), and (3) finite elements (Flood Modeller 2023, HEC-RAS 2017, MIKE 11 2021, Sobek 2018). For all categories, the momentum equation is replaced by an empirical stage-discharge relationships at the location of structures. This approach is equivalent to imposing internal boundary conditions (IBCs) on the nodes where hydraulic structures are located. IBCs allow the representation of various structures (Zhao et al. 1994), including gates (Hernandez et al. 2013), and reduce the need for local mesh refinement (Echeverribar et al., 2019).

The aim of this paper is to present an alternative implementation of IBCs for the representation of hydraulic structures. This aspect is critical to simulate large river systems that are heavily impacted by human activities such as navigation and energy production (Dazzi *et al*. 2020). In classical solution methods the nodes around the structure location must be as close as possible, so that the underlying assumptions of the stage-discharge relationships remain valid. For instance, according to Sobek (2018), adjacent nodes of the structure should be no more than 0.5 m apart. This requires the use of small-time steps to maintain stability around the discontinuity. Therefore, these schemes face significant challenges in providing fast, accurate and stable solutions.

The discontinuous Galerkin (DG) method is a hybrid approach that combines the finite volume and finite element approaches. It also deals with the weak formulation, but it allows the integration of the equations over each segment (in one dimension) or a cell (in two dimensions) independently. The connectivity of each element with its neighbours is ensured by means of numerical fluxes, which are responsible for the transfer of information. Unlike finite volume methods, a higher order approximation to the solution can be applied over each element, making the method less sensitive to the flux treatment applied at the element edges (Draoui *et al*. 2020). Regarding the inclusion of hydraulic structures in water flow modelling, in the DG method, the discontinuities at the boundaries give the possibility of using an alternative approach to that used in classical methods. In this paper, the conventional numerical fluxes are replaced by newly formulated fluxes that allows the application of empirical relationships at the location of structures without the drawback of requiring the sections upstream and downstream of the structure to be very close to one another.

The computational power available nowadays allows not only the simulation of large and complex systems in either one, two or three dimensions, but also their combination in a single model. Therefore, efforts have been made to develop and adapt new integration methods for the shallow water equations; one of which using the discontinuous Galerkin method. Since the introduction of the DG method by Reed and Hill (1973), further developments have been made to deal with shallow water equations (Cockburn *et al*. 1990, Cockburn and Shu 1989, 1998, Kesserwani *et al*. 2008, Kesserwani and Liang 2011). So far, the method has been shown to be useful in situations where the level of detail required to simulate the systems varies depending on the region (de Brye *et al*. 2010), for example, when an inland river system, estuaries, coast, and ocean are coupled. In addition, the method has been tested for natural river systems, demonstrating its ability to handle highly variable bed topography (Lai and Khan 2012), as well as its relevance to channel networks simulation (Neupane and Dawson 2015). However, the viability of the DG approach for water flow in navigable rivers with significant discontinuities has yet to be evaluated.

The SLIM (Second generation Louvain-la-Neuve Ice ocean Model) model used here includes different modules allowing to simulate a range of different water environments: the one-dimensional, the two-dimensional, and the three-dimensional modules (Hanert *et al.* 2023, Ishimwe *et al.* 2023, Saint-Amand *et al.* 2023). When needed the 1D river model can be fully coupled with the 2D model to represent larger water bodies. Such a framework optimizes the computational resources without compromising the accuracy of the flow simulations. Here, the additional structural modules enable us to simulate the influence of hydraulic structures on the flow. The DG method in the current model has several advantages, including high-order accuracy, more flexibility in choosing the numerical flux approximation, and ease of parallelization, which is especially useful when dealing with large domains. In order to demonstrate the robustness of the proposed method for the incorporation of hydraulic structures in this model, the Meuse River and its canal network (Campine Canal) that run through Belgium are chosen as a test case (Figure 1). It corresponds to a highly regulated river system. The structures in this river network are meant to keep a minimum water level that allows continuous navigation year around.

Hydraulic structures used for navigation can play a significant role during extreme flow events. Therefore, it is important to be able to adapt the configuration of the structures in real time to avoid flooding. Most of the studies on the Meuse River have focused on the assessment of the impact on flooding of changes in key factors, such as land use and climate changes (Ashagrie *et al*. 2006, Batlle-Aguilar *et al*. 2007, Leander *et al*. 2005, Tu *et al*. 2005,Wit *et al*. 2001). Furthermore, flood inundation maps for communities along the Meuse River have been generated using a two-dimensional shallow water model to assess flood damage (Beckers *et al*. 2013, Erpicum *et al*. 2010). However, for such shallow water models in situations like flood simulation, the hydrostatic pressure hypothesis applies everywhere, including across the structure. Hence, while the research done involves modelling flow simulations in specific regions for extreme events, it does not address the influence of hydraulic structures in large river system such as the Meuse River and the associated canals. Globally, large-scale hydrodynamic modelling has been applied in various locations, such as the Amazon River (de Paiva et al., 2013), the Yangtze River (Lai et al., 2013), the Paraguay River (Paz et al., 2010) and the Paraná River (Fleischmann et al., 2021). Most of these studies are limited to modelling natural river flows and their interactions with lakes and floodplains. In the study of the Paraná River, dams were considered; however, they are represented within an explicit local inertia method to solve for one-dimensional flow, which lacks the advection term in the momentum equation as considered in the present study (Cozzolino et al., 2019).

Among the canals connected to the Meuse River, the Albert Canal is one of the major waterways and sources of drinking water in Belgium. During low flows in the Meuse River, navigation in the Albert Canal and water supplies are largely compromised. The operation of navigation locks during low flow periods can lead to a drop in water levels. Therefore, the Belgian agency of navigation has been using models to optimize the operation of these structures during both high and low flows (Pereira *et al*. 2016). One of these models is a reservoir-type conceptual model that has been developed to investigate the impact of low flows on water quality under changing climate scenarios (Bertels and Willems 2022). The existing models simulate the structure in a non-explicit manner as a combination of a sink-source by using a time series of observed discharged. However, this approach restricts the extrapolation for periods where no measurements are available. Therefore, the explicit simulation of the structures is believed to be crucial. In previous studies (Pereira *et al*. 2016) in this area, the diversion structures are considered as fixed structures, which may be a reasonable assumption for low to moderate flows. However, in the case of variable flow regimes, a stationary structure will not be sufficient to represent flow distribution between the channel branches. In such conditions, it is essential that the operation of the structures is represented dynamically.

The aim of this paper is firstly to introduce a novel discontinuous Galerkin approach in order to develop a system capable of reproducing the effect of hydraulic structures on the river flow. For that, we expand the SLIM (www.slim-ocean.be) modelling framework by incorporating additional modules for hydraulic structures. Secondly, the model is developed with the aim to simulate both low and high flows for large navigation water systems such as the Meuse River systems. For this, a method is used to represent the operation rules of these structures in the river. We assess these new developments by comparing flow simulations in the Belgian Meuse River and canal systems against measurements. Finally, once the simulation capabilities of the model are demonstrated, it is further used to analyse the impact of the structure's operation on the river discharge and discharge distribution in the canal network. Such large-scale system capabilities, together with process-based models, are crucial for sediment transport and water quality studies.

2. Materials and Methods

2.1 Numerical Modelling: Implementation of hydraulic structures

The DG approach has several benefits when simulating flow and transport in rivers with sudden changes in flow induced by, for example, hydraulic structures. Under such conditions, the hydraulic structures in the DG Method can be implemented by imposing a discontinuity at the location of the structure. At this point, rather than employing the typical flux approach in which flow variables in the shallow water equations is computed using the Riemann problem solver, a stage-discharge relationship for the structure is employed, as shown in Figure 2. Refer to Appendix 1 for the explanation of the DG approach used to solve the shallow water problem using numerical flux obtained by Riemann solvers.

Using the stage-discharge relationship, the discharge across the structure is calculated based on the computed area on element Ω_e and Ω_{e+1}. Accordingly, the flux term is calculated as follows, where the negative sign in the matrix for $F|_{U_2^e}$ is indicative of the flow direction:

$$F|_{U_1^{e+1}} = \begin{bmatrix} Q_{stage} \\ \frac{Q_{stage}^2}{A_1^{e+1}} \end{bmatrix} \text{and } F|_{U_2^e} = \begin{bmatrix} -Q_{stage} \\ -\frac{Q_{stage}^2}{A_2^e} \end{bmatrix} \quad (1)$$

where, Q_{stage} is the discharge calculated using the stage-discharge relationship, and A_1^{e+1} and A_2^e are the computed areas on the nodes downstream and upstream of the structure, respectively. The above Eq. 1 indicates that the flow across the structure can be entirely based on the water level and velocity observed upstream and downstream of the structure. In this implementation, the classic standard structures and their stage-discharge relationships determined empirically have been incorporated.

2.1.1 Stage-Discharge Relationships

The discharge over a weir is determined as a function of the difference in water levels. Based on the construction of the weir, the relationship between the stage and discharge can vary. Rectangular broad crested weirs are considered in this study, which are most prevalent in river systems. In this type of structure, the expression for discharge will depend on upstream water level (H_{us}), the weir crest level (h_w) and the downstream water level (H_{ds}) (Figure 3).

Under these conditions, two scenarios are possible. In the first case, the downstream water level is low enough that it has no effect on the upstream flow conditions (free flow condition), whereas in the second case, the downstream water level is high enough to affect the upstream discharge and water level (submerged flow conditions). The equation for weirs is represented in Eq. 2 (Bos, 1989):

$$Q_{stage} = \begin{cases} C_1 W(H_{us} - H_w)\sqrt{(H_{us} - H_w)} \;\; for \;\; \frac{(H_{ds} - H_w)}{H_{us}} < \frac{2}{3} \; Free\ flow \\ C_2 W(H_{ds} - H_w)\sqrt{(H_{us} - H_{ds})} \;\; for \;\; \frac{(H_{ds} - H_w)}{H_{us}} \geq \frac{2}{3} \; Submerged\ flow \end{cases} \quad (2)$$

where, C_1 and C_2 = weir coefficient; and W = width of the structure (see Figure 7 for the width representation). The above Eq. 2, when applied to submerged conditions, allows connecting the upstream water level of element Ω_e to the downstream water level of element Ω_{e+1} across the structures. As a result, no special treatment of the water level is required for the direct implementation in the discontinuous Galerkin method. In the above Eq. 2, the upstream water level typically is always greater than the weir crest. However, a zero discharge is computed across the weir if the water levels upstream and downstream are lower than the weir crest.

Sluice gates are widely used to control the discharge from rivers into canals. If the gate opening is unsubmerged or in free flow conditions, then relationship will only depend on the upstream water level and gate opening. If the opening is submerged, the discharge also depends on the submergence depth (H_{us}/H_{ds}) (Figure 4). The relevant equations for computing the discharge is represented in Eq. 3 (Bos, 1989):

$$Q_{stage} = \begin{cases} CWH_w\sqrt{2gH} \;\; Where\ H = H_{us} - H_w \; for \; \frac{H_{us}}{H_{ds}} < 0.6667, \; Free\ Flow \\ CWH_w\sqrt{2g3H} \; Where\ H = H_{us} - H_{ds} \; for \; \frac{H_{us}}{H_{ds}} > 0.6667, \; Submerged \end{cases} \quad (3)$$

where, H_w = gate opening height and C = the loss coefficient. In the sluice gate, several other possibilities such as submerged weir flow can also occur but is not considered in this study.

2.2 Model Setup

The Meuse River follows a transboundary course in Europe for up to 905 km in length (Beckers *et al*. 2013). It originates in France and flows through Belgium to reach the North Sea through the Netherlands. The case study area comprises the Meuse River in Belgium and the canal networks to which it is connected. The 143 kilometres long stretch of the Meuse River considered here runs from the Belgian-French border to Maastricht in the Netherlands. The Meuse River is connected to Albert Canal and Zuid-Willemsvaart Canal, which are included in the model. The former extends over 130 kilometres from the Meuse River to the port of Antwerp, and the latter runs over 46 kilometres from Maastricht to Lozen. Interconnections between these main canals play an important part in water distribution (spans around 130 km). As a result, the canals that connect the Albert Canal, such as Bocholt-Herentals, Schoten-Dessel, Kwaadmechelen-Dessel and Briegdan-Neerharn are also included in the computational domain. A section of the Juliana Canal, just downstream of its connection with the Meuse River, is also represented in the simulations. For the description of the river-canal system refer to Appendix 2. The domain of the study is shown in Figure 5.

The Meuse River, collects runoff from a basin of approximately 35,000 km^2, of which 16,670 km^2 is located upstream of Liege (Lambert et al., 2017). Most of this lies in the Walloon region of Belgium, and the low mountain range of the Ardennes is where it gets the most precipitation. The Meuse is mainly a rain-fed river. The river flow shows significant temporal variability, ranging from low flows of about 50 m^3/s during dry summer periods to high flows of about 3000 m^3/s during wet winter periods (Ward et al., 2008)

2.2.1 Meuse River Model: Setup

The cross-sectional profile of the riverbed is required to solve the Saint-Venant equations. The bathymetric data (multi-beam sonar) is combined with the topography data (LidAR) to improve the representation of the riverbanks. This is because the LiDAR's are unable to fully penetrate the water and the fact that sonars are often employed in boats prevents them from covering the banks. The topography, however, can stretch far enough from the riverbanks. An illustration of this is shown in Appendix 3.

Discharge at upstream boundaries of the computational domain is prescribed at three locations, as shown in Figure 5:

- at the measurement station of Chooz, which is located close to the French-Belgian border,
- at Ronet on the Sambre river (left-bank tributary of river Meuse)
- and at Sauheid on the Ourthe river.

These rivers are the only tributaries for which bathymetric data are available; hence, they are included in the model up to the first available discharge measurement point upstream their corresponding confluence. For the rest of the tributaries, no bathymetric data is available. In order to include the flow delivered by the tributaries, available time series of discharge measured upstream at the confluence with the river Meuse are introduced into the model as source terms at the junction, as shown in Figure 5. The stations used for specifying the source terms representing the tributaries are listed in Table 1.

For the downstream boundaries, the water levels measured at (1) Wijnegem station located in Albert Canal, (2) Boergerhan station in Juliana Canal, (3) Boergerhan dorp station in Meuse River and (4) Lozen station in Zuid-Willemstraat canal are used.

2.2.2 Canal Model: Setup

In the Campine canal, it is considered that the slope of the channels between lock chambers is negligible. This is based on the historical information presented in the reports, where the elevation downstream of a lock chamber is identical to the elevation upstream of the following lock chamber. Additionally, due to a lack of precise bathymetry, the cross section of the canals is assumed to be rectangular. For the width of the channel ortho-photos are used from (“Geopunt Flanders” 2022). The structures, such as bypass channels and culverts used to maintain the water level, are also adjacent to each lock. Other smaller canals lack bypass channels and rely solely on culverts to keep the water level constant. For information regarding operating principles refer to Appendix 2. Since there is a lack of data on how these structures function, it is difficult to establish precisely how each of them would affect the flow. As a result, addressing the unknown factors of each structure independently in the numerical model can result in a variable space with large number of dimensions that could not be defined adequately. Therefore, we deal with them as single input-output structures, where the different flows (the flow through bypass, culverts and leakage losses) through them are lumped. Here, these structures are implemented as a weir for the sake of simplicity and to further avoid the complications of the simulation of the emptying and filling of the lock chamber. The simulation of the emptying/filling time of a lock chamber requires a smaller simulation time step. The important advantage to simulate lock chamber as weirs is that weirs make possible both regulation of the water level and the control of the discharge flow through the structure.

Downstream the Belgian-Dutch border, the connection between the Meuse River and the Zuid-Willemsvaart canal at Maastricht is simulated as an sluice gate. The dimensions of the sluice gate are based on in situ measurements, and the gate opening is determined to approximate a discharge of 11 m^3/s. Moreover, there will be a steady discharge through the gate because the Zuid Willemsvaart canal lock at Bocholt and the weir at Maastricht control the water level upstream and downstream of the sluice gate, respectively. As a result, the Meuse River is set up to discharge approximately 11 m^3/s of water into the main canal, which is consistent with reported data (Van Steenbergen 2017, De smedt and Van der beken 1982).

2.2.3 Operation Rules for the Weirs.

The operation of the weirs in the Meuse River is such that the water level upstream remains at a target value, which is based on the discharge flow regime (high or low flow). All weirs along the Meuse River follow these operation rules, except for the Monsin Weir, where the target water level remains constant regardless of flow regime. This is due to the position of this weir in the direct vicinity of the bifurcation with the Albert Canal just upstream of the weir. The target water level can be clearly observed in the measurement data (see Appendix 2); the level of the weir crest, on the other hand, cannot be estimated nor any measurement data is available to the authors. Additionally, as illustrated in Figure 6, weirs are divided in the lateral direction of the flow and the radial gates can be operated individually. Thus, it is possible to obstruct the flow in some weirs while passing it through others. If so, no data regarding this operation is available. Hence, we assume that all the gates of the weir are always in operation and the width of these gates are determined using ortho-photos.

Due to this data limitation, implementing these operation rules is a difficult task. Nonetheless, based on field data Eq. 4 was obtained in order to compute the weir crest level (h_w):

$$h_w = h_m - \left(\frac{Q}{C_1 w}\right)^{3/2} \tag{4}$$

where, h_m is the water that needs to be maintained. This equation is directly derived from the weir equation. If the parameters such as weir coefficient and width (w) are kept constant, the weir crest will mainly depend on hm and discharge Q. The constant water level that needs to be maintained can be determined from data, and the weir crest level can then be controlled solely by discharge. In the model, this discharge is obtained from a node upstream of the weir. In general, the operations rules that are employed in the model will allow all the discharge to pass through the weir. This can be seen as an inverse problem where, based on the discharge and water level the elevation of the crest level is determined.

2.2.4 Calibration Method

In the shallow water equations, the computed flow variables are the cross-sectional flow area and the discharge. Two model parameters must be estimated by calibration. One is the Manning coefficient associated with flow resistance modelling, and the other is the weir coefficient in the stage-discharge relationships characterizing the structures. A dependence of such coefficients on flow variability (e.g. hysteresis in the stage-discharge relationship) may arguably exist. However, this dependence is only strong for extreme conditions such as low water depth (Garcia 2005) or flooding (Perret et al. 2022).

The model is assessed by comparing the numerical results against measured water levels and discharges recorded at gauging stations. Most existing stations record water levels and only a few of them also monitor discharge. The model for the Meuse River is calibrated in two steps. First, the weir coefficients and the Manning coefficients are calibrated for a fixed elevation for the crest of the weirs. This situation happens during low flow periods when the weirs are barely operated, and inflows from the catchment and tributaries are minimal. Time series of water levels and discharges during such periods are used for a first estimation of the value of each coefficient. In this step, the simulated discharges are compared with observations at Waulsort and Anseremme stations (Figure 10). In a second step, a longer time series that comprises low and high flow periods is used to further fine tune the coefficients. During this period of time the weirs are operated in accordance with their regulation equations. In this step, the computed water levels are compared to measurements at Anseremme station (Figure 11). Figure 7 illustrates the flow chart for the steps involved in the method of calibration that is then used for the validation of flow variables at a different period.

The Nash-Sutcliffe Efficiency (NSE) coefficient is used as a metrics for model performance (Moriasi *et al*. 2007). In particular cases in which the observations remain almost constant in time (e.g., regulated water level), the performance reported by the NSE coefficient is artificially low, as a result of the definition of this metrics (Morales-Hernández *et al*. 2013). Hence, an additional performance metrics is utilized. It consists in evaluating the percentage of simulated data that fall within the 95% confidence interval of the observations (based on the standard deviation of the observations) (Van Liew *et al*. 2003)

2.3 Data Availability

Among the data available, the majority of it consists of data collected by the measuring station for water level and discharge. Besides that, data such as the bathymetry of the river and the description of the canal are also made available by the regional authorities. In this section, all the measured data and the relevant data that are used during model setup, validation and calibration are described.

2.3.1 Bathymetric data

The elevation data used to extract the cross-sectional profiles was provided by the 'Service Public de Wallonie' (SPW), the regional authority for the Meuse River. The bathymetric data for the Meuse River were collected using multi-beam sonars and in certain shallow water areas by echo sounders with a resolution of 10 cm. The relief of the flood plains was measured using the airborne LiDAR technique with a resolution of 1m. Unfortunately, a detailed bathymetric information for the Campine canal is not available. However, due to the regularity of the cross-section and the presence of locks, it is possible to construct the longitudinal profile of the canal. This is achieved by using information about the geometric characteristics of locks (FHR,2005) and high resolution ortho-photos.

2.3.2 Meuse River

In the Meuse River most of the stations that record the water level are situated immediately upstream of the weirs. Additionally, the difference in water levels between upstream and downstream of the weir is large enough to prevent submersion of the structure. Therefore, water levels observed at these stations are around a target water level that guarantees navigability along the river. However, in the case of the Lixhe station, the measurements are done (shown in Figure 5) directly downstream the last weir used for navigation in the Belgian Meuse. The calibration of the model is done using the measurement of the water level at Anseremme. With regards to the model validation, we compare the simulated water levels against measurements done at

Anseremme, GRD and at Lixhe.

The model is also calibrated and validated for discharges. Although five measurement stations exist, four of them have sufficient historical data for these purposes. The four stations are: (1) Chooz, whose measurements are used as a boundary condition, (2) Amay, the only station in the upper Meuse, (3) Waulsort, located downstream Chooz and (4) Eijsden, located in the lower Meuse (Figure 5). Though the Waulsort station has a record for short time series, it is selected for the calibration because this includes a phase of low flows that was adequate for the approach followed in the first step of calibration (Section 2.2.4). Perhaps more importantly, this station is the closest to the upstream boundary thus minimizing the effect of surface runoff. The time series for all these measurements in the Meuse River were obtained from “Service public de Wallonie” for Belgium and “Rijkswaterstaat” for the Netherlands. The measurement station used in this study for validation and calibration is shown in Figure 5.

2.3.3 Campine Canal

The Albert Canal, as previously stated, begins at the junction with the Meuse River. The amount of discharge that is fed into the canal is determined by the operation of the weir in Monsin. The discharge required for canal operation has been reported in several publications (De smedt and Van der beken 1982, FHR 2005, Van Steenbergen 2017) and is also measured in the Albert Canal at the diversion. Table 2 describes the discharge reported by these studies at two different locations. One, at Monsin, where the division occurs and secondly, at Genk, where the first lock in Albert Canal is placed.

The literature data on discharge reports single values and therefore they do not take into account the flow fluctuation in the Meuse River. The reported figures, shows discharges that vary within the range of 16 and 25 m^3/s. However, the measurement values from the Haccourt station, located nearby the bifurcation of the Meuse into the Albert Canal, and Kanne station, which is closest to the Albert Canal's first lock (Genk), both show negative discharges (Figure 8). Furthermore, the measurements at these stations show that the discharge can reach 100 m^3/s (Figure 8), even when the discharge recorded in the Meuse River at Amay station is around 50 m^3/s. This could be attributed to interferences in the measurements taken at these locations (e.g., effect of waves induced by vessels, lock operations). The influence of lock operation is more significant at the Kanne measuring station, which is because of its proximity towards the lock. As a result of these effects, the direct use of these measurements for calibration and validation is not possible because the model does not include these phenomena. Nonetheless, the average trend of the time series could give us some insight about the water flow.

The other Campine canals exhibit a similar behaviour as that of stations in the Albert Canal. The interference due to operation in this case is much larger due to its closer proximity to the lock chamber. As a result, the measurement data does not provide reliable information on the discharge. However previous studies by (De smedt and Van der beken 1982) were able to measure an average discharge distribution across the Campine channel. For the water level measurements, the reported data in the literature agrees well with the measurement data. Additionally, in Albert Canal, there are water level measurements taken at Marxhe, which is located immediately after the bifurcation, as shown in Figure 5. Therefore, in order to validate the implementation of diversion structures in the Meuse River for the Albert Canal, Marxhe Station is taken into account. The rest of the canal networks has over 20 water level measurement locations, each positioned just upstream of the lock chamber. Not all of these locations are used for validation; instead, the measurements closest to the bifurcation within these canals are selected. All the measurement stations used for validation for the water levels in the Albert Canal and the Campine canals are shown in Figure 5.

3. Results and Discussion

3.1 Meuse Model

Here, the results of model simulation compared to a standard software Mike 11 are shown (section 3.1.1), then the results of the two-step calibration procedure introduced in Section 2.2.4 are presented (section 3.1.2), followed by additional comparisons between computations and observations aiming at validating the model (section 3.1.3). An overview of all measured data considered for model calibration and validation is given in Table 3. The validation includes several stations along the stretch of the river with different durations, to illustrate the robustness of the model.

3.1.1 Comparison with MIKE 11 model

To evaluate the structure implementation in SLIM, the model results are compared to those of the model MIKE11. The Meuse River domain, which includes three weirs, is used for the comparison up to around 20 km from the French-Belgian border (Figure 1). A steady discharge of 105 m^3/s is applied at the upstream boundary and a water level of 91.1 m at the downstream boundary, as measured in Chooz and Dinant. The weir heights are computed using the approach outlined in Section 2.2.3 for steady state conditions. Figure 9 shows the comparison of water level and velocity computed by both models. The present model results agrees with the outcomes of MIKE11 model, demonstrating the validity of the implementation. However, certain variations in velocity are due to differences in mesh resolution.

3.1.2 Calibration: Meuse Model

As a first step in calibration method described in section 2.2.4, the simulated discharge at Waulsort, and water level at Anseremme is compared to measurements done between May 10 and May 21, 2021 (Figure 10). In the second step, the weir coefficient was further improved; here, the results were compared to those of water levels measured at Anseremme between June 4 and December 31, 2019 (Figure 11).

Figure 10 shows a comparison of the simulated and measured discharges at Waulsort and Anseremme. In both cases, the NSE coefficient is equal to 0.94 and the confidence interval covers 99% of the total simulated data in the first step of calibration. During the calibration, it is observed that lower weir coefficients (<1.6) result in a rise in water level (greater than measured) due to hold up of the flow. Furthermore, a first estimation of Manning coefficient of 0.033 $s/m^{1/3}$ yielded satisfactory results. It is worth noting that the chosen Manning coefficient for the first estimate is based on the range of coarse sand and gravel bed (Arcement and Schneider, 1989). It can be seen in Figure 10, the calibrated results closely follow the main trend of the observation time series. Moreover, in comparison to measured data, the model has a deficit in the cumulative volume of around 1% (presumably due to surface runoff coming from urban area and inter-catchment not included in the model), which indicates that the model preserves the water volume and provides good prediction in comparison to measured data.

In the second step, the water level between the measurement done at Anseremme and the simulated values are compared (Figure 11): the NSE coefficient is 0.74 and a confidence interval with coverage of 96% is achieved. In this step, the weir coefficient is further increased to 1.8 to minimize hold up with respect to high flows. Several Manning coefficients (0.028, 0.03, and 0.033 $sm^{-1/3}$) were applied to fine-tune the coefficients, but no substantial difference in results was seen, hence 0.033 $sm^{-1/3}$ was retained from the first step. Therefore, weir coefficient of 1.8 and Manning coefficient of 0.033 $sm^{-1/3}$ were found to fit best with the measured values (irrespective of high or low flow) and was used in all subsequent simulations. It can be seen (Figure 11) that the calibrated simulation closely follows the main trend of the observation time series. However, it does not catch the fluctuations around the mean flow. Precipitation in the inter-catchment basin of the Meuse River, from Chooz to Waulsort, including tributaries, may be a cause of such fluctuations. Moreover, the station being close to the weir and lock chamber can record the waves generated and propagated by the structures, potentially causing the water level to fluctuate.

3.1.3 Validation: Meuse Model

In the validation, as described in section 2.3.2, the comparison of simulated water levels and discharge to measurements are presented. The first three figures (Figure 12a, 12b and 13) show the water levels and last two figure (Figure 14 and 15) shows the discharge.

The comparison of water levels at Anseremme between the model and measured values (Figure 12a) has a NSE coefficient of 0.68 and 95% of the simulations are covered by the confidence interval. For the water level comparison at GRD, the NSE coefficient is 0.65, and the confidence interval covers 93% of the simulation (Figure 12b). The sudden shift in water level observed, especially in the case of Anseremme (Figure 12a: ~1000 hour) is because the operations of the weirs, as simulated by the model, are instantaneous, while in reality, the operation of the weir takes place gradually. In the case of GRD, for a period of around 16th November 2019 (i.e., 4000th hour in Figure 12b), a difference between simulated and measured water levels is observed. The details behind this behaviour are unknown to the authors, but this is most probably due to the operation rules. However, after the lower point of the observations, the model matches again the target level.

The next water level measurement station is located in Lixhe, which is further downstream from the bifurcation of the Meuse River into Albert Canal. The NSE coefficient for the comparison of water levels between the model and measured data is 0.93, and the confidence interval covers 96% of the simulations (Figure 13). The behaviour of water level time series in this station is different from what was observed in rest of the upstream stations. Here, the influence of the operation rules is minimal, and changes are dependent only on the flow. Therefore. a relatively higher NSE coefficient compared to other two stations are achieved. Moreover, as mentioned in section 2.2.4, the NSE coefficients tend to stay artificially low for time series like Anseremme and GRD.

As discussed in section 2.3.2, in the upper Meuse, Amay is the only suitable station for the validation of discharge with sufficient historical values. The comparison between the simulated and measured discharges for Amay station is shown in Figure 14. A NSE coefficient of 0.92, a cumulative deficit equal to 4.3% and coverage of 98% were obtained (Figure 14). These performance evaluators show a good agreement between simulation and measured flow. However, differences can be seen for some discharge peaks. The primary reasons for this are the inflows into the river during high precipitation events, not only coming from the Meuse catchment but also from the catchment of the tributaries. Moreover, some of the discharge measurement stations are not placed near the confluence of the tributary with the Meuse River but a few kilometres upstream. This makes it difficult to estimate the arrival time of a flood event and thus the contribution to the peak discharges in the Meuse River.

Similar results with an NSE coefficient of 0.96 and 97% coverage can be seen for the comparison of discharge between simulated and measurements done at Eijsden station (Figure 15). It can be seen that the representation of the peaks and their arrival time are well simulated by the model. In comparison with Amay station, the model results show better results in Eijden (since they consider different periods). This further indicates that these differences in peaks are caused by a lack of monitoring stations for the influx of water into the river.

To summarize the model performance Figure 16a provides an overview of the NSE values obtained during the calibration and validation steps of the model, while Figure 16b reports the portion of computed values falling outside the confidence interval of the measurements.

The NSE coefficients and confidence intervals for the comparison of the simulated and measured values indicates a good model performance. However, the NSE coefficient measured for water levels in Anseremme during validation is lower than that achieved during calibration. This is justified by the fact that the amplitude range of the oscillations is larger, with a mean of 15 cm against 10 cm during the calibration period. While, for the discharge comparison the NSE values are greater than 0.9 and values out of confidence interval increases for the measurements located further downstream the river, primarily due to lack of inputs form the lateral inflows. Although the NSE coefficient by nature tends to undermine the model performance at Anseremme and GRD, values outside of the confidence interval that are well below 7% reaffirm the model's capability.

3.2 Canal system

In Sub-section 3.2.1, the focus here is set on evaluating the performance of the model for predicting the discharge partition between the Meuse River and the Albert Canal, with the aim of validating our implementation of the diversion structure controlling this flow partitioning. Next, computed water levels in the canals are compared to observations in Section 3.2.2, while Section 3.2.3 discusses the model ability to reproduce the discharge distribution between various canal branches.

3.2.1 Discharge partition between the Meuse River and the Albert canal

For evaluating our implementation of the diversion structure controlling the flow at the bifurcation between the Albert Canal and the Meuse River (Monsin weir), measurements at Marxhe station are considered over a period of six months (between June 1, 2013 and December 31, 2013, as shown in Figure 17a). The simulated and measured time series show a good agreement for the water level, with a maximum deviation of 0.12 m. Figure 17b compares the simulated discharge entering the Albert Canal to the measured discharges at Haccourt during the same six-month period. Although the discharge measurements show inaccuracies, as discussed in Section 2.3.3, the simulated results follow the overall trend of the measured time series. Simulated discharge peaks appear fairly consistent with the higher values in the observations, in spite of the presence of high-frequency disturbances in the measured time series. During normal flow in the Meuse River (from 100th until 3000th hour in Figure 17b), the simulated discharge in the Albert Canal is between 12 and 31 m^3/s. The differences in the reported data (De smedt and Van der beken, 1982; FHR, 2005; Van Steenbergen, 2017) for estimated values of discharge all fall within this range. This shows that the simulated discharges are consistent with the values reported in literature. Such model capabilities are made possible thanks to the regulation rules implemented in the model to reproduce the influence of Monsin weir.

3.2.2 Water levels

Figure 18 displays computed and measured water levels at six stations in the Albert Canal and the Campine canals. The simulated water levels are in good agreement with the measured data. The error magnitudes on the mean value remains below 1 cm at half of the stations (Genk, Kwaadmechelen and Mol), while they reach 2 cm, 5 cm, and 7 cm at stations Rijkevorsel, Grobendonk and Bocholt, respectively (Table 4). Furthermore, the mean values of the simulated results correspond to the value indicated in the literature data (FHR, 2005)

The fluctuations in the measured water levels differ substantially from one station to the other. In the Albert Canal at Genk, Kwaadmechelen and Grobendonk, the amplitude of the fluctuations reaches 0.30 m, whereas they are about twice smaller (~ 0.17 m) in the other Campine canals. This difference is consistent with the larger capacity of the lock chambers in the Albert canal (transfer of ~ 5×10^4 m^3 per lock operation (FHR, 2005)) compared to the locks in other canals, which is likely to lead to higher amplitudes of the waves induced by lock operations. Again, the simulations do not resolve these waves since individual lock operations are not reproduced in the model, which leads to maximum absolute differences between simulated and measured water levels as presented in Table 4.

3.2.3 Discharge partition between canal branches

The simulated distribution of discharge in the Campine canal connected to the Meuse River is shown in Figure 19. The minimum and maximum values of discharge presented in Figure 19 corresponds to months from June to August 2013. The discharge in the Meuse River shows an average of about 400 m^3/s and a minimum value of 40 m^3/s at Monsin. These simulated values are close to observations reported in a previous study

(De smedt and Van der beken 1982) that are described in section 2.3.3.

High discharges in the Meuse River have a significant influence on the flow in the Albert Canal, where the discharge can reach 90 m^3/s (three times the average value), as can be seen in Figure 17b. In the Campine canal, the impact is less significant. This is mainly due to the high regulation of the water inflow into the Zuid-Willemsvaart canal through an sluice gate and a weir in Maastricht. In the Dessel-Kwaadmechelen canal (Figure 5), during high flow events in the Albert Canal, the flow direction is reversed. The impact is larger here than along the other two canals (Dessel-Schoten and Bocholt-Herentals) connected to the Albert canal because the locks placed along them regulate the flow at the connection.

3.3 Influence of the modelling of operation rules

As the operation rules of the hydraulic structures along the Meuse River are incompletely documented, their modelling in this study relies on assumptions derived from measured data. However, inferring operation rules from data interpretation remains challenging. Therefore, we test here the sensitivity of modelling results to the operation of weirs in the simulations. Two modelling options were tested. In Scenario 1, the weirs are assumed to be mobile, as they actually are. In Scenario 2, the weirs are assumed to be set at a fixed position, corresponding to the lowest probable value of their crest elevation. Scenario 1 is run first, and the position of the weirs were recorded. Then, the lowest position of each weir was selected to be used as fixed position in Scenario 2. Unlike scenario 1, it is evident that water levels will fluctuate in scenario 2. As illustrated in Figure 20b, for scenario 2 the water level at the weir increases during the rise in discharge (230–325 hours in Figure 20a), whereas for scenario 1 it remains constant. However, the impact of this on discharge in the far reach of the river is examined (in this case, near Eijsden).

As shown in Figure 20a, the time series of discharges are very similar between the two scenarios, suggesting that the operation rules of the weirs have limited influence on the peak discharges in the Meuse River. In Scenario 1, the peak discharge arrives 1-2 hours earlier than in Scenario 2 and the peak discharge is about 15 m^3/s higher than in Scenario 2. In the rising limb of a flood wave (for example, between the 230th and 263rd hours), Scenario 2 lags behind Scenario 1, whereas during the recession part, the results of both scenarios can hardly be distinguished. This is consistent with the stronger backwater effects occurring in the case of fixed weirs (Scenario 2) compared to the case of mobile weirs (Scenario 1). Indeed, in Scenario 1, the lowering of the weirs as the discharge rises minimizes delays of the flood wave due to storage. Nonetheless, the delays and changes in peak magnitude are not substantial due to the limited storage capacity of the Meuse River itself. The implementation of floodplains in the model would lead to more water storage; but it would still remain limited to a few percents (Kitsikoudis *et al*., 2020)

4. Conclusion

This study implements empirical relationships to model hydraulic structures within a discontinuous Galerkin finite element model for open-channel flow, applied to the Belgian section of the Meuse River and its connected canals. The model demonstrates stability under transient conditions and achieves good agreement with field measurements, with NSE coefficients ranging from 0.65 to 0.78 for water levels and 0.9 to 0.95 for river discharges . Additionally, over 92% of the results fall within the 95% confidence interval. Within the canal system, the simulated water levels showed a good agreement with errors on the mean value of the water level ranging from 1 to 7 cm. While the model effectively captures the main hydrodynamic processes influenced by the structures, it underestimates the peak flows highlighting the challenge of limited flow measurements, which affects the inflow estimates. In addition, there are some discrepancies in water levels due to unaccounted factors such as wind-induced waves, navigation effects, and lock operations.

The DG method is thus validated for its capability to handle different hydraulic structures, such as weirs and sluice gates. The results show that the numerical approach for structures ensures correct calculation of the discharge across the structures, while keeping the upstream water level above the crest of the weir. Moreover, the model shows good stability for dynamically operated structures. In terms of model setup, the mesh resolution around the structure becomes less important, due to the characteristics of the DG method.

The developed model proves to be an effective tool for understanding the intricate effects of the hydraulic structures on discharges and water levels in complex channel networks. Consequently, this model can assist in the development of control algorithms that can effectively integrate the operation of multiple structures. In addition, flow simulation can be valuable in calculating sediment erosion/deposition and for pollutant transport in such large systems.

To better represent the peaks, a hydrological model should be coupled to the developed hydrodynamic model to reduce uncertainties related to inflows along the channels. Additional discharge measurements would also provide more opportunities for detailed model validation. If waves induced by individual operations of structures such as locks need to be predicted, data on boat traffic should be included in the model.

Acknowledgements.

This research was carried out in the framework of doctoral fellowship PO4500049108, which is awarded to the first author of the present article and is funded by the Engie

Electrabel and Belgian Nuclear Research Centre (SCK·CEN). The work was carried out in SCK·CEN and Université catholique de Louvain and is thankful for the resources provided. The authors are also grateful to Prof. Sandra Soares Frazao (UC Louvain, Belgium) and Dr. Luc Moens (UC Louvain, Belgium) for fruitful discussion regarding the model. Thanks, are also due to Marie Lahaye for providing contact information and Maryse Vercammen (Service public de Wallonie mobilité et infrastructures) for sharing available information regarding the structures in the Meuse River. The authors are also thankful to members of SLIM team who contributed to the development of the present model.

Disclosure statement

The authors report there are no competing interests to declare.

References

Arcement, G.J. and Schneider, V.R., 1989. Guide for selecting Manning's roughness coefficients for natural channels and flood plains. USGS Numbered Series 2339. U.S. Geological Survey, https://doi.org/10.3133/wsp2339.

Ashagrie, A.G. *et al.*, 2006. Detecting the influence of land use changes on discharges and floods in the Meuse River Basin - the predictive power of a ninety-year rainfall-runoff relation?, *Hydrology and Earth System Sciences*, 10(5), 691–701. https://doi.org/10.5194/hess-10-691-2006.

Batlle-Aguilar, J. *et al*., 2007. Identification of groundwater quality trends in a chalk aquifer threatened by intensive agriculture in Belgium, *Hydrogeology Journal*, 15, 1615–1627. https://doi.org/10.1007/s10040-007-0204-y.

Beckers, A. *et al*., 2013. Contribution of land use changes to future flood damage along the river Meuse in the Walloon region, *Natural Hazards and Earth System Sciences*, 13(9), 2301–2318. https://doi.org/10.5194/nhess-13-2301-2013.

Bertels, D. and Willems, P., 2022. Climate change impact on salinization of drinking water inlets along the Campine Canals, Belgium, *Journal of Hydrology: Regional Studies*, 42, 101129. https://doi.org/10.1016/j.ejrh.2022.101129.

Bos, M.G., 1989, Discharge measurement structures.

de Brye, B., *et al*., 2010. A finite-element, multi-scale model of the Scheldt tributaries, river, estuary and ROFI, *Coastal Engineering*, 57(9), 850–863. https://doi.org/10.1016/j.coastaleng.2010.04.001.

Cockburn, B., Hou, S., and Shu, C. W., 1990. The Runge-Kutta Local Projection Discontinuous Galerkin Finite Element Method for Conservation Laws. IV: The Multidimensional Case, *Mathematics of Computation*, 54(190), 545–581. https://doi.org/10.2307/2008501.

Cockburn, B., and Shu, C. W., 1989. TVB Runge-Kutta Local Projection Discontinuous Galerkin Finite Element Method for Conservation Laws II: General Framework, *Mathematics of Computation*, 52(186), 411–435. https://doi.org/10.2307/2008474.

Cockburn, B. and Shu, C. W., 1998. The Runge–Kutta Discontinuous Galerkin Method for Conservation Laws V: Multidimensional Systems, *Journal of Computational Physics*, 141(2), 199–224. https://doi.org/10.1006/jcph.1998.5892.

Cozzolino, L., *et al*., 2019. Flood Propagation Modeling with the Local Inertia Approximation: Theoretical and Numerical Analysis of Its Physical Limitations, *Advances in Water Resources*, 133, 103422, https://doi.org/10.1016/j.advwatres.2019.103422.

Dazzi, S., Vacondio, R., and Mignosa, P., 2020. Internal boundary conditions for a GPU-accelerated 2D shallow water model: Implementation and applications, *Advances in Water Resources*, 137, 103525. https://doi.org/10.1016/j.advwatres.2020.103525.

De smedt, F., and Van der beken, A., 1982. Het transport van conservatieve stoffen in het Albertkanaal en de Kempische kanalen. Available from: https://www.vliz.be/imisdocs/publications/ocrd/33/241133.pdf.

Draoui, I. *et al*., 2020. Discontinuous Galerkin method for 1D river flows. *In*: Proceedings of the 10th Conference on Fluvial Hydraulics, 7-10 July 2020 Delft: 1114–1121. https://doi.org/10.1201/b22619-156.

Erpicum, S., *et al*., 2010. Detailed Inundation Modelling Using High Resolution DEMs, *Engineering Applications of Computational Fluid Mechanics*, 4(2), 196–208. https://doi.org/10.1080/19942060.2010.11015310.

FHR, 2005. Watersysteem van het albertkanaal en de kempense kanalen. MOD 720/4. Flander Hydraulic Research. Available from: https://www.vliz.be/imisdocs/publications/35/140435.pdf. [Accessed 10 February 2023]

Fleischmann, A. S., *et al*., 2021. Regional Scale Hydrodynamic Modeling of the River-Floodplain-Reservoir Continuum, *Journal of Hydrology*, 596, 126114, https://doi.org/10.1016/j.jhydrol.2021.126114.

Flood Modeller, 2023. Flood Modeller Technical Reference. Flood Modeller (Reference Manual). Available from: https://help.floodmodeller.com/docs/1d-modelling-theory-overview.

García, R., 2005. Analysis of Manning coefficient for small-depth flows on vegetated beds. Hydrological Processes, 19, 3221–3233. https://doi.org/10.1002/hyp.5820

García-Alén, G., et al., 2021. Modelling Weirs in Two-Dimensional Shallow Water Models, Water, 13(16), 2152. https://doi.org/10.3390/w13162152.

'Geopunt Flanders', 2022. Available at: www.geopunt.be.

HEC-RAS, 2017. HEC-RAS River Analysis System. US army Corps of Engineers (Reference Manual). Available from: https://www.hec.usace.army.mil/software/hec-ras/documentation/HEC-RAS%205.0%20Reference%20Manual.pdf.

Hodges, B.R., 2013. Challenges in Continental River Dynamics, *Environmental Modelling & Software*, 50, 16–20. https://doi.org/10.1016/j.envsoft.2013.08.010.

Iserles, A., 2008. A First Course in the Numerical Analysis of Differential Equations. 2nd edn. Cambridge: Cambridge University Press (Cambridge Texts in Applied Mathematics). https://doi.org/10.1017/CBO9780511995569.

Kesserwani, G., *et al*., 2008. Application of a second-order Runge–Kutta discontinuous Galerkin scheme for the shallow water equations with source terms, *International Journal for Numerical Methods in Fluids*, 56(7), 805–821. https://doi.org/10.1002/fld.1550.

Kesserwani, G., and Liang, Q., 2011. A conservative high-order discontinuous Galerkin method for the shallow water equations with arbitrary topography, *International Journal for Numerical Methods in Engineering*, 86(1), 47–69. https://doi.org/10.1002/nme.3044.

Kitsikoudis, V., *et al*., 2020. Discrepancies in Flood Modelling Approaches in Transboundary River Systems: Legacy of the Past or Well-grounded Choices?, *Water Resources Management*, 34(11), 3465–3478. https://doi.org/10.1007/s11269-020-02621-5.

Lai, W., and Khan, A.A., 2012. Discontinuous Galerkin Method for 1D Shallow Water Flows in Natural Rivers, *Engineering Applications of Computational Fluid Mechanics*, 6(1), 74–86. https://doi.org/10.1080/19942060.2012.11015404.

Lai, X., *et al*., 2013. Large-Scale Hydrodynamic Modeling of the Middle Yangtze River Basin with Complex River–Lake Interactions, *Journal of Hydrology*, 492, 228–43, https://doi.org/10.1016/j.jhydrol.2013.03.049.

Lambert, T., *et al*., 2017. Effects of Human Land Use on the Terrestrial and Aquatic Sources of Fluvial Organic Matter in a Temperate River Basin (The Meuse River, Belgium), *Biogeochemistry*, 136(2), 191–211, https://doi.org/10.1007/s10533-017-0387-9.

Leander, R., *et al*., 2005. Estimation of extreme floods of the River Meuse using a stochastic weather generator and a rainfall–runoff model / Estimation des crues extrêmes de la Meuse à l'aide d'un générateur stochastique de variables météorologiques et d'un modèle pluie–débit, *Hydrological Sciences Journal*, 50(6), 1103. https://doi.org/10.1623/hysj.2005.50.6.1089.

MIKE 11, 2021. A Modelling System for Rivers and Channels. Mike 11 (Reference Manual). Available from: https://manuals.mikepoweredbydhi.help/2021/Water_Resources/Mike_11_ref.pdf.

Morales-Hernández, M., Murillo, J., and García-Navarro, P., 2013. The formulation of internal boundary conditions in unsteady 2-D shallow water flows: Application to flood regulation, *Water Resources Research*, 49(1), 471–487. https://doi.org/10.1002/wrcr.20062.

Moriasi, D., *et al*., 2007. Model Evaluation Guidelines for Systematic Quantification of Accuracy in Watershed Simulations, *Transactions of the ASABE*, 50. https://doi.org/10.13031/2013.23153.

Neupane, P., and Dawson, C., 2015. A discontinuous Galerkin method for modeling flow in networks of channels, *Advances in Water Resources*, 79, 61–79. https://doi.org/10.1016/j.advwatres.2015.02.012.

de Paiva, R. C. D., *et al.*, 2013. Large-Scale Hydrologic and Hydrodynamic Modeling of the Amazon River Basin, *Water Resources Research*, 49(3), 1226–43, https://doi.org/10.1002/wrcr.20067.

Paz, A. R., *et al*., 2010. Large-Scale Hydrodynamic Modeling of a Complex River Network and Floodplains, *Journal of Hydrologic Engineering*, 15(2),152–65, https://doi.org/10.1061/(ASCE)HE.1943-5584.0000162.

Pereira, F., *et al*., 2016. Verlaging van de waterstanden in het Albertkanaal juli 2011. WL2016A14_074_1. Antwerp: Hydraulic Engineering Laboratory. Available from: http://www.vliz.be/imisdocs/publications/ocrd/26/290826.pdf

Perret, E., Lang, M., and Le Coz, J., 2022. A framework for detecting stage-discharge hysteresis due to flow unsteadiness: Application to France's national hydrometry network. *Journal of Hydrology*, 608, 127567. https://doi.org/10.1016/j.jhydrol.2022.127567

Quarteroni, A., Sacco, R., and Saleri, F., 2007. Principles of Numerical Mathematics. Berlin, Heidelberg: Springer, pp. 33–56. https://doi.org/10.1007/978-3-540-49809-4_2.

Reed, W.H., and Hill, T.R., 1973. Triangular mesh methods for the neutron transport equation. LA-UR-73-479; CONF-730414-2. Los Alamos Scientific Lab., N.Mex. (USA). Available from: https://www.osti.gov/biblio/4491151 [Accessed: 13 October 2023].

Sobek, 2018, 1D/2D modelling suite for integral water solutions. Deltares (Reference Manual), Available from: https://www.deltares.nl/en/software/sobek/.

Toro, E.F., 2009. Riemann Solvers and Numerical Methods for Fluid Dynamics: A Practical Introduction. Berlin, Heidelberg: Springer.

Tu, M. *et al.*, 2005. Extreme floods in the Meuse River over the past century: aggravated by land-use changes?, *Physics and Chemistry of the Earth*, 30(4), 267–276. https://doi.org/10.1016/j.pce.2004.10.001.

Van Liew, M., Arnold, J., and Garbrecht, J.D., 2003. Hydrologic Simulation on Agricultural Watersheds: Choosing Between Two Models, *Transactions of the American Society of Agricultural Engineers*, 46, pp. 1539–1551. Available at: https://doi.org/10.13031/2013.15643.

Van Steenbergen, N., 2017. Low water in the Albert Canal: You've got to pump it up!, Available from: https://publicwiki.deltares.nl/display/HydrologyMeuse/4th+symposium+on+the+hydrological+modelling+of+the+Meuse+basin?preview=/130387019/130387164/vanSteenbergen_Youvegottopumpitup.pdf [Accessed: 28 March 2023].

Ward, P. J., *et al.*, 2008. Strong Increases in Flood Frequency and Discharge of the River Meuse over the Late Holocene: Impacts of Long-Term Anthropogenic Land Use Change and Climate Variability, *Hydrology and Earth System Sciences*,12(1), 159–75, https://doi.org/10.5194/hess-12-159-2008.

Wit, M.J.M. de *et al.*, 2001. Effect of Climate Change on the Hydrology of the River Meuse. Dutch National Research Programme on Global Air Pollution and Climate Change. NRP. Available at: https://research.wur.nl/en/publications/effect-of-climate-change-on-the-hydrology-of-the-river-meuse [Accessed: 28 March 2023].

Zerihun, Y.T., and Fenton, J.D., 2007. A Boussinesq-type model for flow over trapezoidal profile weirs, *Journal of Hydraulic Research*, 45(4), 519–528. https://doi.org/10.1080/00221686.2007.9521787.

Appendix

1 Discontinuous Galerkin Method

Typically, river has a length relatively greater than its width. This is why a one-dimensional numerical model is appropriate. Such a model solves the shallow water equations in order to provide water flow variables averaged over each cross section of the river. This study uses the 1D discontinuous Galerkin method (DG) in the framework of SLIM to solve the Saint-Venant equations. These equations express the conservation of volume and momentum in terms of cross-sectional area and discharge as follows:

$$\frac{\partial}{\partial t}\begin{bmatrix} A \\ Q \end{bmatrix} + \frac{\partial}{\partial x}\begin{bmatrix} Q \\ \frac{Q^2}{A} + \frac{P}{\rho} \end{bmatrix} = \begin{bmatrix} s \\ -gA\frac{\partial h}{\partial x} - gAS + \frac{F}{\rho} \end{bmatrix} \quad \text{(A1)}$$

where, Q and A represent the volumetric flow rate and cross-sectional area, s is the source term used to include tributaries, t is the time, x is the stream-wise coordinate, h represents the water depth to the deepest point in the cross section, P is the hydrostatic pressure force and F is the along-flow component of the pressure force resulting from the width variation.

S is the slope of the energy line (i.e., the friction induced head loss per unit distance) and the Manning formulation for S (A, Q) is given by:

$$\mathrm{S} = \mathrm{n}^2 \frac{\mathrm{Q}|\mathrm{Q}|}{A^2(\mathrm{H}^*)^{4/3}} \quad \text{(A2)}$$

with $H^* = A/b^*$ the hydraulic radius, b^* is the free surface width and n is the Manning coefficient.

Conservation Eq. A1 are solved by approximating the solution using the discontinuous Galerkin (DG) method. The main characteristic of this method is that it applies the finite element method for the integration of the shallow water equation at element level independently. However, this situation leads to multiple solutions at the inter-element interfaces. Therefore, a unique solution is determined by using numerical fluxes (also known as Riemann Solvers) as done in the finite volume method approach. Thus, the DG method is normally seen as a combination of both approaches.

To illustrate this method, consider the above Saint-Venant equations in their generalized form:

$$\frac{\partial U}{\partial t} + \frac{\partial F(U)}{\partial x} = S(U) \tag{A3}$$

where U is the vector of unknowns with A and Q, whilst the $F(U)$ and $S(U)$ are the fluxes and source terms, respectively. In order to approximate the solution, the computational domain Ω is divided into a set of N_e non-overlapping elements Ω_e (Figure A1).

Based on the generalized form, U can be approximated as U_h in the finite dimensional space of polynomials on element Ω_e, with φ the set of independent shape functions and U_i^e the new unknown nodal values. The approximate solution for each element is written as follows:

$$U|_{\Omega_e} \simeq U_h|_{\Omega_e} = \sum_{i=1}^{2} \phi_i U_i^e \tag{A4}$$

In the next step the weak formulation is obtained by multiplying Eq. A3 by the local basis functions φ. Integrating this over Ω_e we obtain the following element solution:

$$\int_{\Omega_e} \frac{\partial U}{\partial t} \varphi_i dx - \int_{\Omega_e} F . \frac{\partial \varphi_i}{\partial x} dx + [F\varphi_i]_{x_e}^{x_{e+1}} = \int_{\Omega_e} S\varphi_i dx \tag{A5}$$

The local boundary term $[F(U)\varphi_i]_{x_e}^{x_{e+1}}$ is the term that connects each element Ω_e with its neighbors. However, due to the discontinuous representation, the variables are double valued at the interface between elements. Consequently, it is important to appropriately define a common variable for U. This is made possible by tackling the Riemann problem, whose solution can be used to calculate these variables at a single discontinuity point using the values on the left and right. The description of the problem contains the mathematical character of physical conservation rules. Here, the Riemann problem is defined for the two adjacent nodes U_2^e and U_1^{e+1} of the neighboring elements. In this method, the conservative equations are transformed on the basis formed by the eigenvectors of the Jacobian matrix for the flux $J = \frac{\partial F(U)}{\partial U}$ to obtain the following characteristic form:

$$\begin{bmatrix} \frac{\partial W1}{\partial t} \\ \frac{\partial W2}{\partial t} \end{bmatrix} + \begin{bmatrix} \frac{Q_0}{A_0} - \sqrt{\frac{gA_0}{b^*}} & 0 \\ 0 & \frac{Q_0}{A_0} + \sqrt{\frac{gA_0}{b^*}} \end{bmatrix} \begin{bmatrix} \frac{\partial W1}{\partial x} \\ \frac{\partial W2}{\partial x} \end{bmatrix} = \begin{bmatrix} -gA\frac{dh}{dx} + gS \\ gA\frac{dh}{dx} - gS \end{bmatrix} \quad \text{(A6)}$$

where A_0 and Q_0 are the mean values between the left U_2^e and U_1^{e+1} nodal values, and W*1* and *W2* are the Riemann invariants. The solution to the Riemann problem for such discontinuity point lies between the characterises of the two eigenvalues (Toro, 2009), and this region is usually known as the star region (*U**). Based on these Riemann invariants the final solution for the Riemann problem is developed, where the variables of U* can be determined by the following equations:

$$\begin{cases} on\ \Omega_e\ -A^*\left(\frac{Q_0}{A_0} + \sqrt{\frac{gA_0}{b^*}}\right) + Q^* = -A_2^e\left(\frac{Q_0}{A_0} + \sqrt{\frac{gA_0}{b^*}}\right) + Q_2^e \\ on\ \Omega_{e+1}\ A^*\left(-\frac{Q_0}{A_0} + \sqrt{\frac{gA_0}{b^*}}\right) + Q^* = A_1^{e+1}\left(-\frac{Q_0}{A_0} + \sqrt{\frac{gA_0}{b^*}}\right) + Q_1^{e+1} \end{cases} \quad \text{(A7)}$$

Consequently, the term $[F(U^*)\varphi_i]_{x_e}^{x_{e+1}}$ is computed along the element edges. Toro (2009) provides a detailed description and relevance of every term in the Riemann problem method. Refer to (Draoui *et al*., 2020) for a thorough description of the method used to implement the DG method for Saint-Venant equations used in the SLIM Model. For the time integration, we employ an implicit Runge-Kutta scheme that allows flexibility in terms of time step (Iserles, 2008; Quarteroni *et al*., 2007).

2 Meuse River Systems

The Belgian part of the Meuse River is highly regulated by a combination of weir systems and lock chambers, which play a major role in river flow dynamics. Along the

Meuse River in Belgium, there are 15 weirs between Givet and Lixhe. These weirs raise the water level to obtain a sufficient hull for navigation even during dry periods. This also aids in reducing the velocities in the river for safer navigation. Beside the weirs, a lock is placed at the same location, which assist the vessel with vertical movement in order to pass from one river segment to the next.

2.1 Structures in Meuse River systems

The weirs in the Meuse River are movable, and they are operated to maintain a target water level in the river. The ooperation of these weirs is based on feedback from water level measuring stations. Furthermore, the river discharge measurements at Chooz in the upper Meuse and Amay in the lower Meuse are also used as complementary criteria for the operation of the weirs. If the discharge in the river reaches a certain threshold, the target water level that needs to be maintained is lowered. This can be observed in measurement data; for instance, as seen in Figure A2a, the measured water level at Anseremme (about 24 kilometres from Chooz) is lowered from 90.35 to 90.06 meters at around 12th December 2019 (i.e., 4650th hours in Figure A2). While at the same time, as seen in Figure A2b, the corresponding discharge measured in Chooz has exceeded the 500 m^3/s discharge threshold. This is done in order to prevent the weir directly upstream of the weir under consideration from becoming submerged.

Nonetheless, in specific locations, such as weirs near major cities like Namur and Liège, the weirs operate under specialized rules. The weir at Liège (referred to as Monsin Weir) is placed in the Meuse just downstream of the splitting point of the Meuse and the Albert Canal (Figure A3a). This weir has the main function to control the flow into the Albert Canal. However, it also plays a significant role in flooding control in the Albert Canal. The Monsin weir can be lifted to function simultaneously as a weir and an sluice gate. Moreover, the structure can be completely lifted during very high flow events to obtain a more effective flow conveyance and avoid flooding the cities. A similar weir is also present in the river at the bifurcation of the Meuse at Maastricht. At the point of water diversion at Maastricht, a weir is used to keep the water level for navigation and to convey the water through the Juliana Canal. Upstream of this bifurcation on the left bank of the Meuse River an sluice gate and lock chamber are used to feed water into the Zuid-Willemsvaart canal (Figure A3b) and to allow navigation through it.

2.2 Structures in Albert Canal and Campine Canals

Figure A4 shows the lock chambers present in the Albert and the Campine canals, which in total comprises 28 locks. Among them, the Albert Canal consists of six locks, each bounded at both ends by a set of three lock chambers, as shown in Figure A5. The navigation in this canal allows larger vessels than in the other canals of the country. The smaller Campine canals, fed by the Zuid-Willemsvaart canal, are connected to the Albert Canal at four different places, as seen in Figure A4. These canals are smaller in size, and navigation is made possible by a single lock chamber. Like the Meuse River maintaining the water level in these canals is also of vital importance. For this purpose, there are bypass channels constructed across the lock chamber (Figure A5) that allow the water to flow continuously once the target water level for navigation is reached at each segment of the canal. For the lock chamber placed in the other Campine Canals, the flow continuity is regulated by the culvert used for filling and emptying the lock chamber.

3 Extraction of cross-section profile.

The cross-sectional profile of the riverbed is required to solve the Saint-Venant equations. For this, the topography data and bathymetric data are combined as follows. The point in the topography data with the highest elevation within 50 meters of the riverbank was chosen as the end point for the cross-section profile (Figure A6). Later, among the highest point from left and right of the river the one with a smaller elevation is considered as the maximum elevations for that profile. These profiles were extracted along lines that were perpendicular to the flow, which were generated based on ortho-photos of the river every 500 meters.

Figure Captions

Figure 1: Location map for the flow of transboundary Meuse River in France, Belgium and The Netherlands that is connected to the network of Campine canal in Belgium.

Figure 2: Representation of the nodes in DG method and the treatment of flux by stage-discharge relationships for the imposed discontinuity at the location of hydraulic structure

Figure 3: The schematic of the weir in the river and the terms corresponding to the computation of the discharge in the weir equations.

Figure 4: The schematic of the sluice gate in the river and the terms corresponding to the computation of the discharge in the gate equations.

Figure 5: Map of the section of Meuse River and its canal systems flowing in Belgium: The location of boundary condition and measurement station used in validation and calibration of the model. The tributaries Sambre and Ourthe are considered in the model with appropriate boundary conditions.

Figure 6: Schematic representation of a typical weir in the Meuse River

Figure 7: Flow chart of the model setup procedures used to calibrate the considered independent variables using measurement stations.

Figure 8: Discharge Measurement data at Kanne (Closest to the Lock) in Albert Canal for the 3 months period (left) and the measurements recorded at this station during low flow in the Meuse River (Right)

Figure 9: Model comparison in the Meuse River using the hydraulic structure of the developed SLIM model and the traditional commercial model MIKE11 for (a) water level (left) and (b) velocity (right).

Figure 10: Waulsort discharge and Anseremme water level station: comparison of simulated and measured values with confidence interval for calibration.

Figure 11: Anseremme water level station: comparison of simulated and measured values with confidence interval for calibration

Figure 12: Comparison of simulated and measured values with confidence interval for Validation (a) Anseremme water level station (top) (b) GRD water level station (bottom)

Figure 13: Lixhe water level station: comparison of simulated and measured values with confidence interval for validation

Figure 14: Amay discharge measurements: comparison of simulated and measured values with confidence interval for validation.

Figure 15: Eijsden discharge measurements: comparison of simulated and measured values with confidence interval for validation.

Figure 16: (a) NSE values obtained in the calibration and the validation of the model for the Meuse River. (b) Portion of computed values falling out of the confidence interval of the observations in the calibration and the validation of the model for the Meuse River.

Figure 17: (a) Marxhe measurement station: Comparison of simulated and measured values (top). (b) Simulated discharge into Albert Canal from the Meuse River at Haccourt Measurement station (bottom)

Figure 18: Comparison of simulated and measured values for validation for all water level stations located along the Campine Canal (refer Figure 5 for locations).

Figure 19: Range of discharge distribution among the interconnected canals with the accurate representation of water levels for June till August 2013

Figure 20: (a) Comparison of discharge for a simulation of mobile and immobile structures in the Meuse River (top) (b) comparison of water levels at two weirs (Rivere and Talifer) for low discharge (235th hour) and high discharge (325th hour) to illustrate the rise in water levels due to immobile structures and constant water level for mobile structure (bottom).

Figure Caption for Appendix

Figure A1: Representation of the nodes in DG method with fluxes for solving shallow water equations and their corresponding symbols used for computation.

Figure A2: (a) The Measurement data for water level station at Anseremme (Top) and (b) discharge station at the Chooz (Bottom): Representation of the target level maintained in the Meuse River and shift in target level due to change in flow regime.

Figure A3: (a) Map for the connection of Albert Canal (Left) and (b) Zuid-Willemsvaart (Right) with the Meuse River and the location of locks and weirs near the connection.

Figure A4: Map for the location of locks in Albert Canal, Zuid-Willemsvaart canal and their interconnecting canals.

Figure A5: Schematic diagram of a typical lock chamber in Albert canal with illustration of different flows across the Lock chamber to maintain the water level.

Figure A6: Illustration of the selection of cross-section profile from the bathymetry and topography data: Perpendicular lines drawn on both data sets (left), cross-section profile for both data sets (middle), Combined profile (right)

Figure 1


's-Hertogenbosch
Netherlands
Venlo
Dessel-Schoten
Bocholt-Herentals
Albert Canal
Germany
Maastricht
Belgium
Liege
Meuse
Namur
Charleville Mezieres
Luxembourg
France
Verdun
Commercy
Saint German sur Meuse

Figure 2

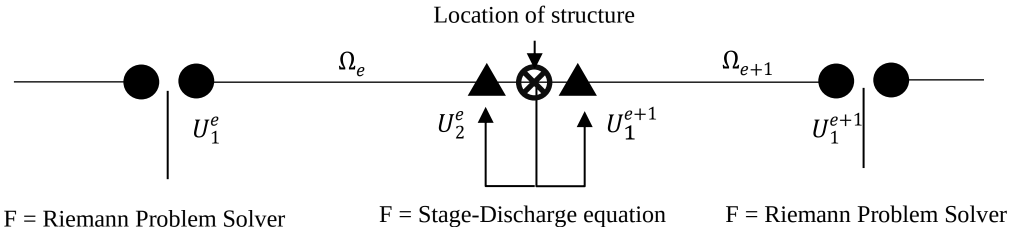
Location of structure
Ω_e
Ω_{e+1}
U_1^e
U_2^e
U_1^{e+1}
U_1^{e+1}
F = Riemann Problem Solver
F = Stage-Discharge equation
F = Riemann Problem Solver

Figure 3

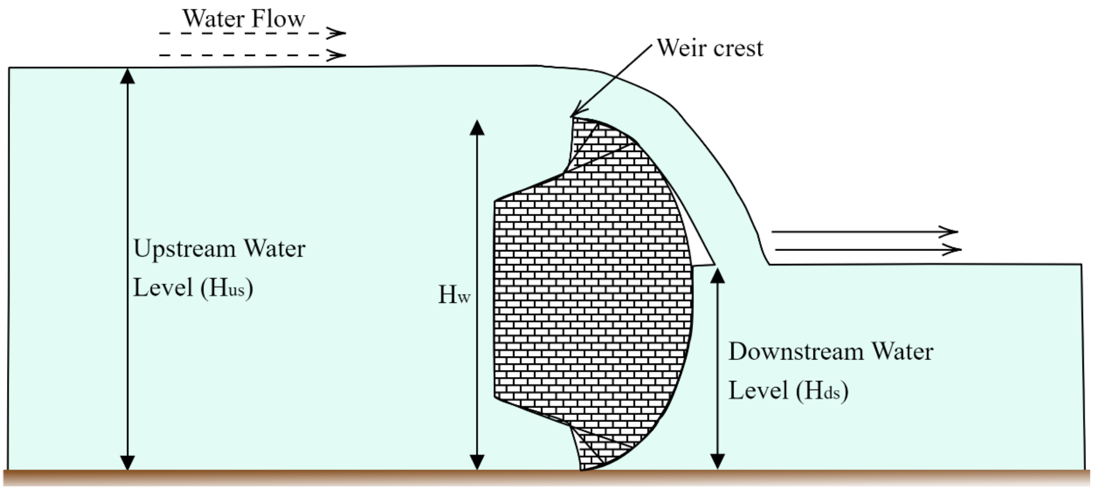

Water Flow
Weir crest
Upstream Water Level (Hus)
Hw
Downstream Water Level (Hds)

Figure 4

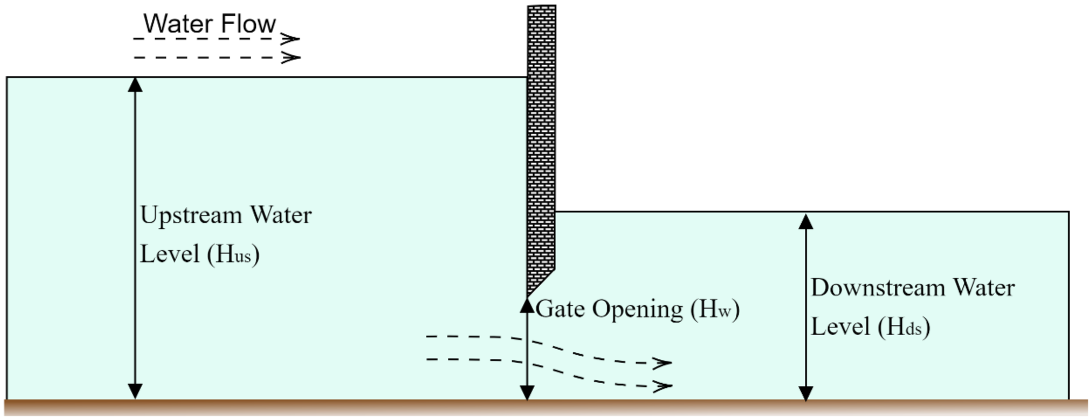
Water Flow
Upstream Water Level (H_{us})
Gate Opening (H_w)
Downstream Water Level (H_{ds})

Figure 5

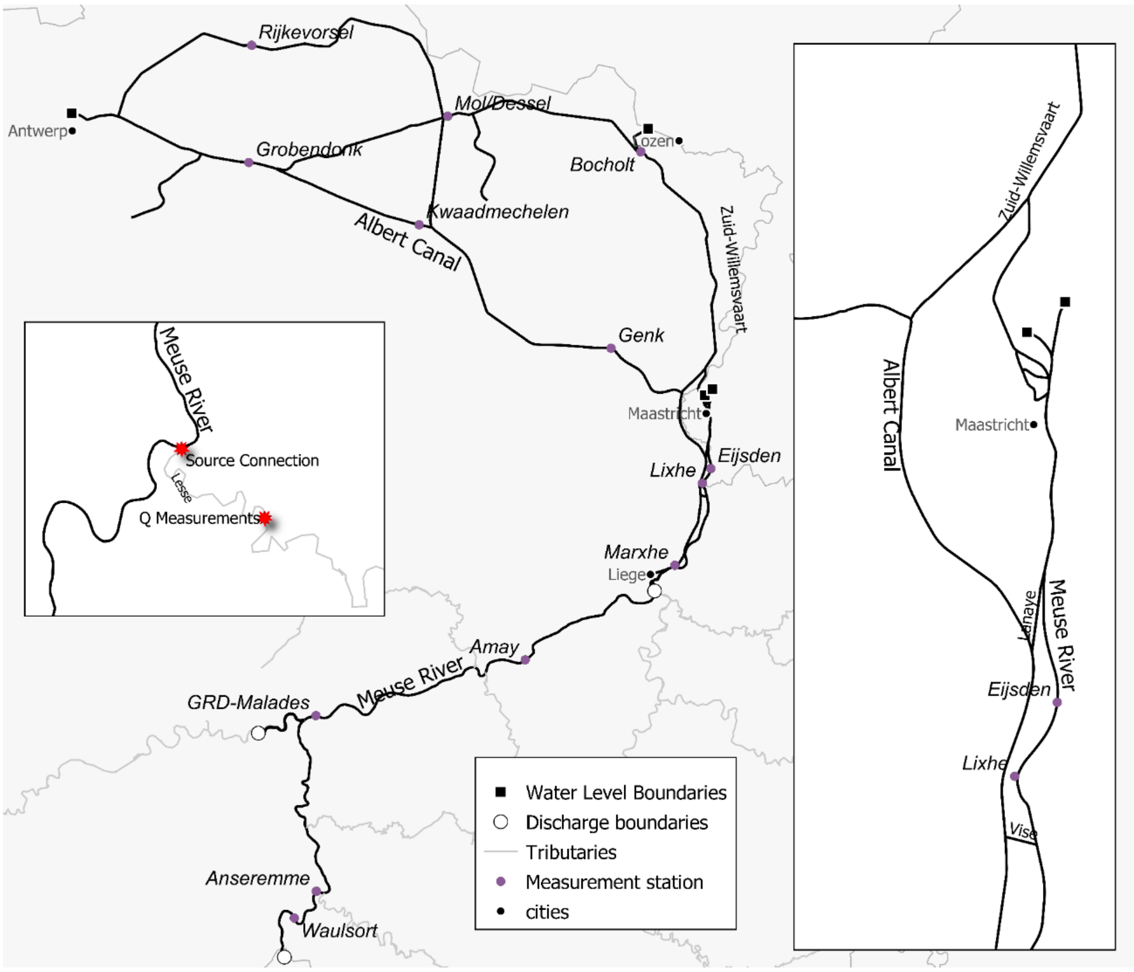

Rijkevorsel
Antwerp
Mol/Dessel
Grobendonk
Lozen
Bocholt
Kwaadmechelen
Albert Canal
Zuid-Willemsvaart
Genk
Maastricht
Eijsden
Lixhe
Marxhe
Liege
Amay
Meuse River
GRD-Malades
Anseremme
Waulsort
Meuse River
Source Connection
Lesse
Q Measurements
Water Level Boundaries
Discharge boundaries
Tributaries
Measurement station
cities
Zuid-Willemsvaart
Albert Canal
Maastricht
Lanaye
Meuse River
Eijsden
Lixhe
Vise

Figure 6

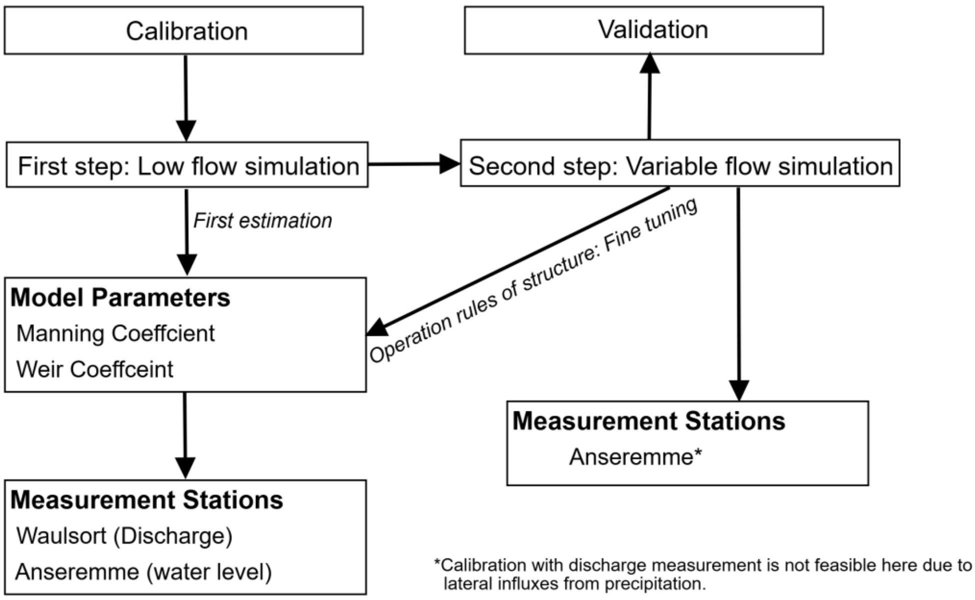
Calibration
Validation
First step: Low flow simulation
Second step: Variable flow simulation
First estimation
Operation rules of structure: Fine tuning
Model Parameters
Manning Coeffcient
Weir Coeffceint
Measurement Stations
Anseremme*
Measurement Stations
Waulsort (Discharge)
Anseremme (water level)
*Calibration with discharge measurement is not feasible here due to lateral influxes from precipitation.

Figure 7

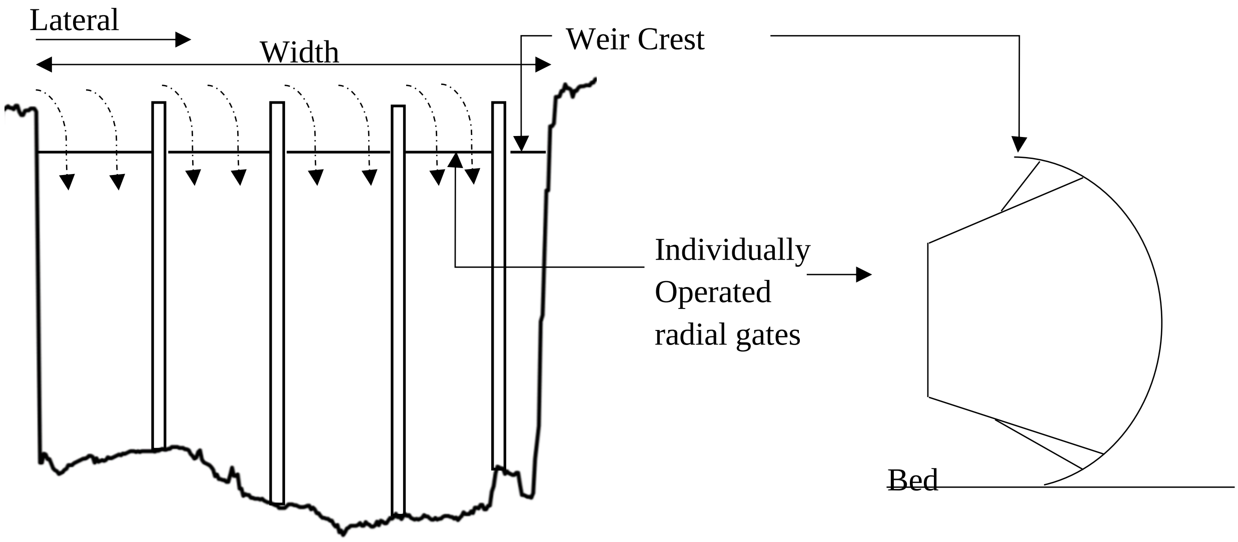
Lateral
Width
Weir Crest
Individually
Operated
radial gates
Bed

Figure 8

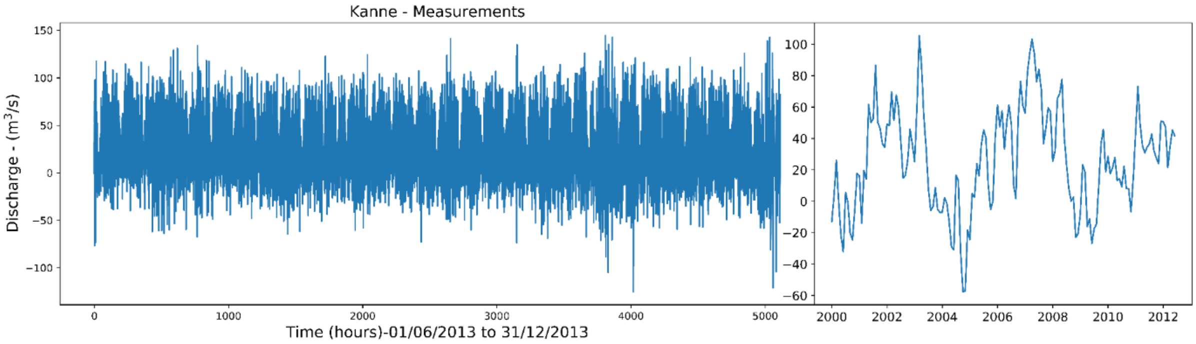
Kanne - Measurements
Discharge - (m³/s)
Time (hours)-01/06/2013 to 31/12/2013
150
100
50
0
−50
−100
0
1000
2000
3000
4000
5000
100
80
60
40
20
0
−20
−40
−60
2000
2002
2004
2006
2008
2010
2012

Figure 9

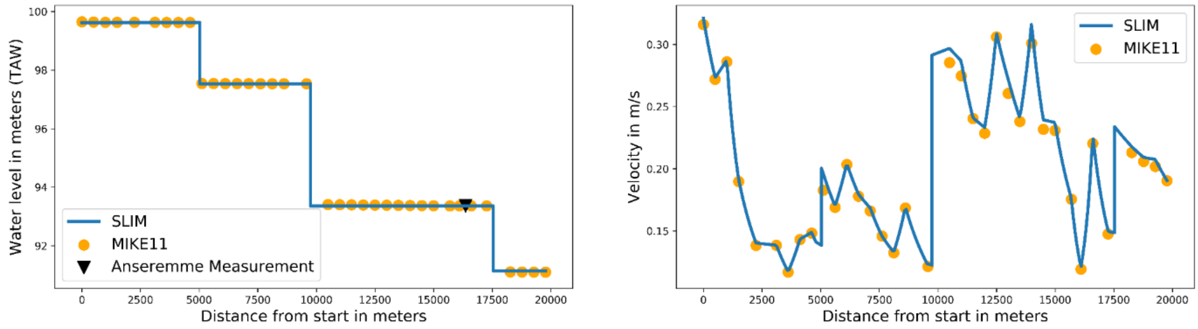
Water level in meters (TAW)
Distance from start in meters
SLIM
MIKE11
Anseremme Measurement
Velocity in m/s
Distance from start in meters
SLIM
MIKE11

Figure 10

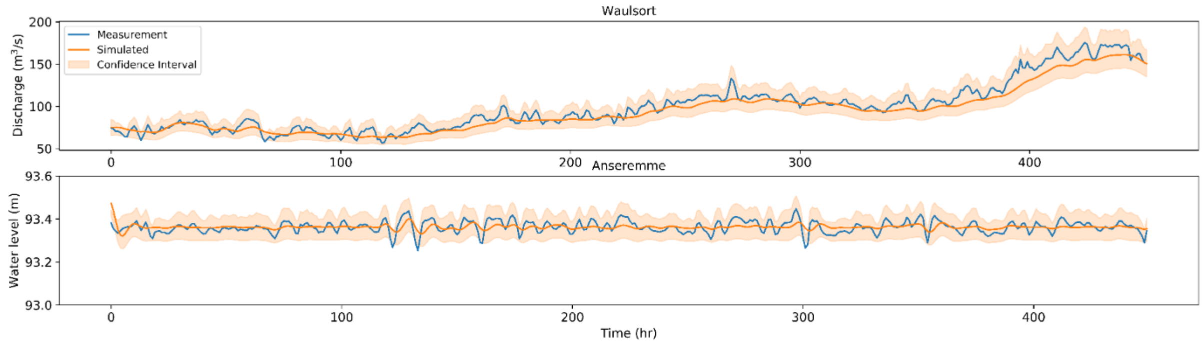
Waulsort
Measurement
Simulated
Confidence Interval
Discharge (m³/s)
Anseremme
Water level (m)
Time (hr)

Figure 11

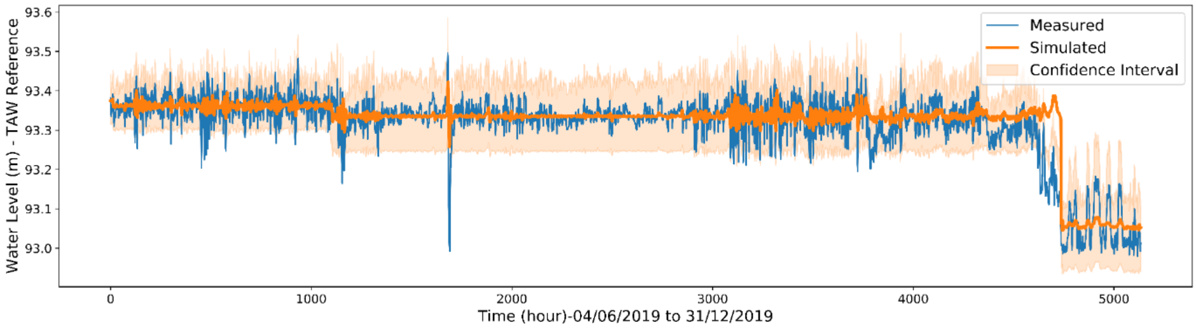
Measured
Simulated
Confidence Interval
Water Level (m) - TAW Reference
93.6
93.5
93.4
93.3
93.2
93.1
93.0
0
1000
2000
3000
4000
5000
Time (hour)-04/06/2019 to 31/12/2019

Figure 12

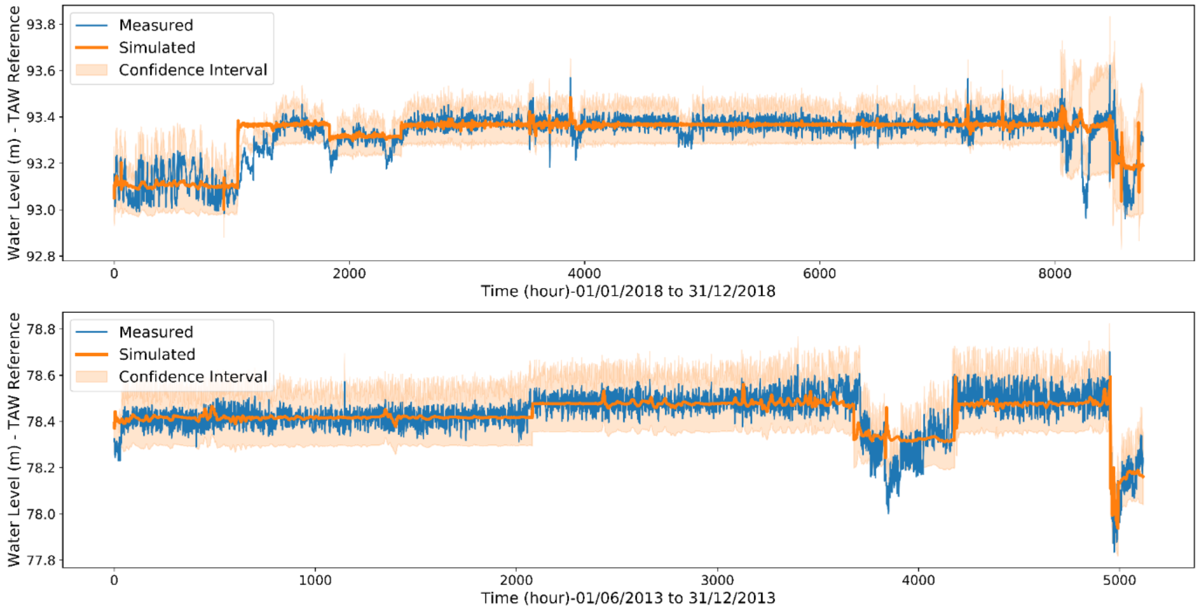
Measured
Simulated
Confidence Interval
Water Level (m) - TAW Reference
93.8
93.6
93.4
93.2
93.0
92.8
0
2000
4000
6000
8000
Time (hour)-01/01/2018 to 31/12/2018
Measured
Simulated
Confidence Interval
Water Level (m) - TAW Reference
78.8
78.6
78.4
78.2
78.0
77.8
0
1000
2000
3000
4000
5000
Time (hour)-01/06/2013 to 31/12/2013

Figure 13

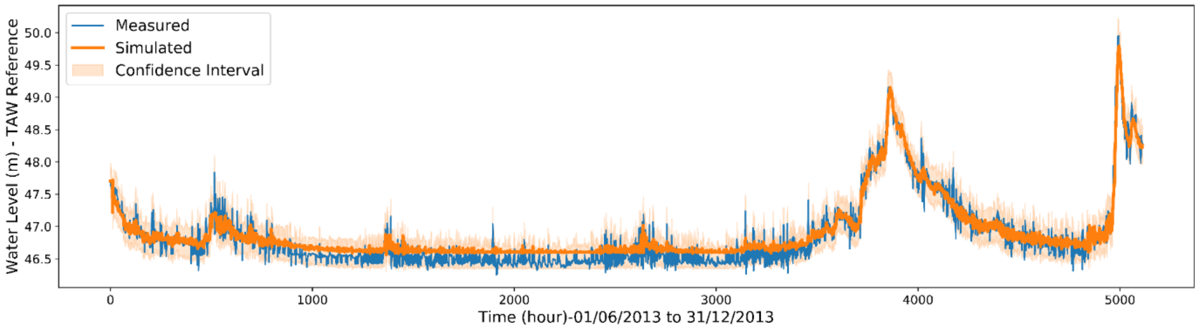
Measured
Simulated
Confidence Interval
Water Level (m) - TAW Reference
50.0
49.5
49.0
48.5
48.0
47.5
47.0
46.5
0
1000
2000
3000
4000
5000
Time (hour)-01/06/2013 to 31/12/2013

Figure 14

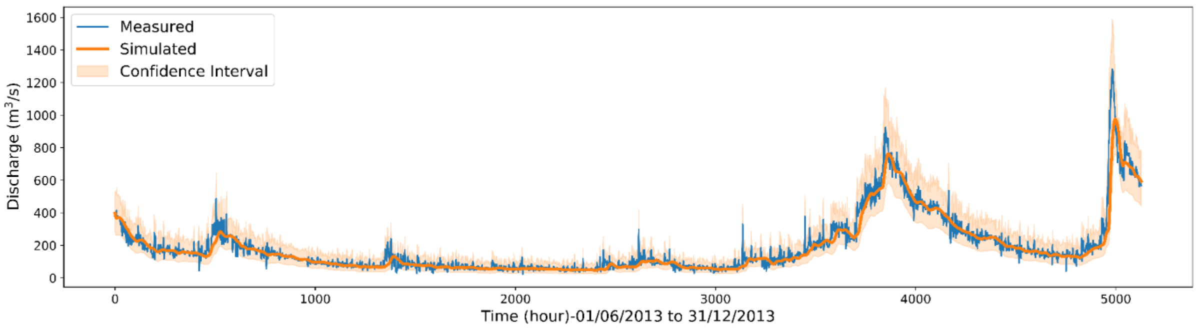
Measured
Simulated
Confidence Interval
Discharge (m³/s)
Time (hour)-01/06/2013 to 31/12/2013
0
200
400
600
800
1000
1200
1400
1600
1000
2000
3000
4000
5000

Figure 15

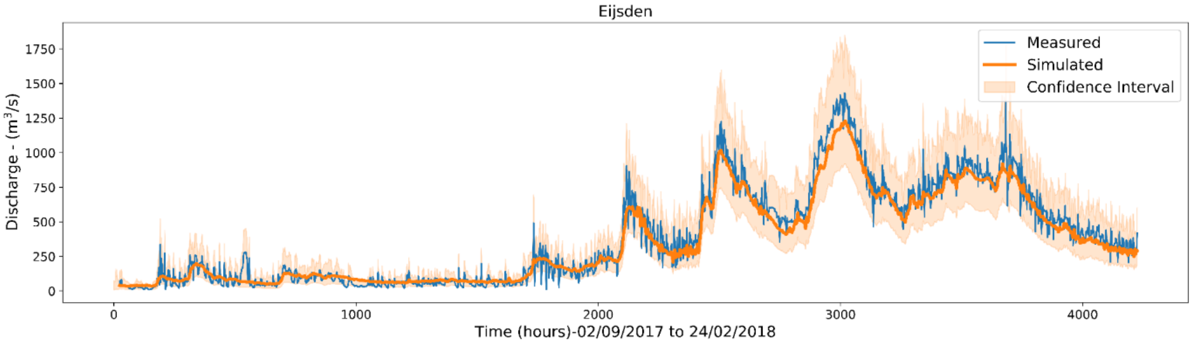
Eijsden
Measured
Simulated
Confidence Interval
Discharge - (m³/s)
Time (hours)-02/09/2017 to 24/02/2018
0
250
500
750
1000
1250
1500
1750
0
1000
2000
3000
4000

Figure 16a

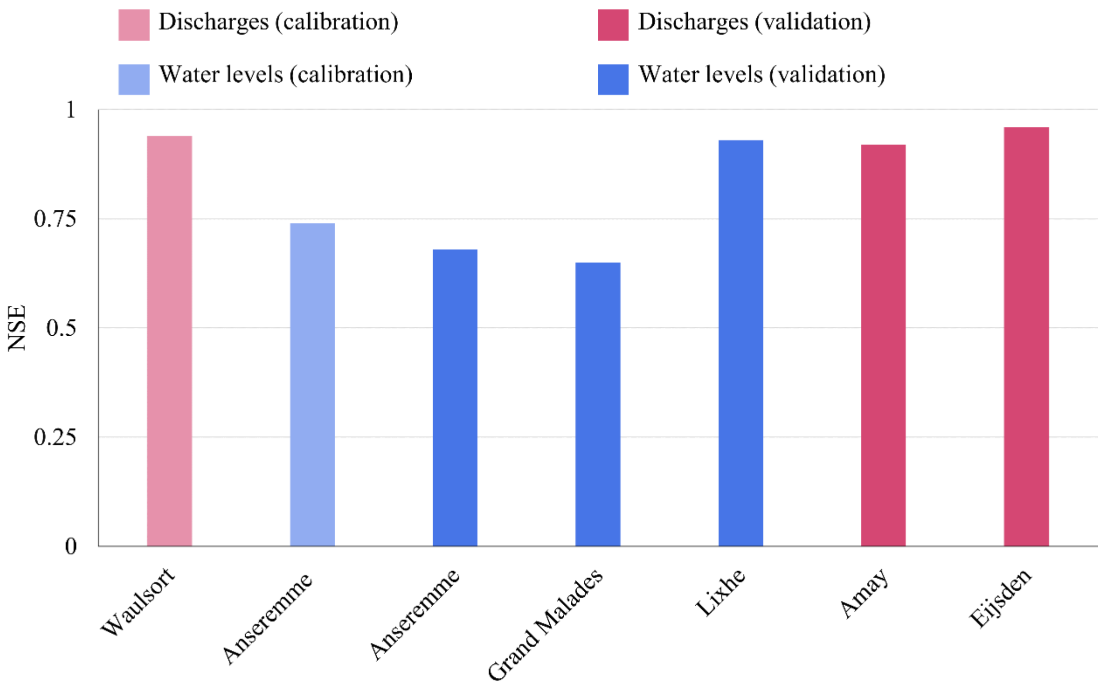

Discharges (calibration)
Discharges (validation)
Water levels (calibration)
Water levels (validation)
NSE
1
0.75
0.5
0.25
0
Waulsort
Anseremme
Anseremme
Grand Malades
Lixhe
Amay
Eijsden

Figure 16b

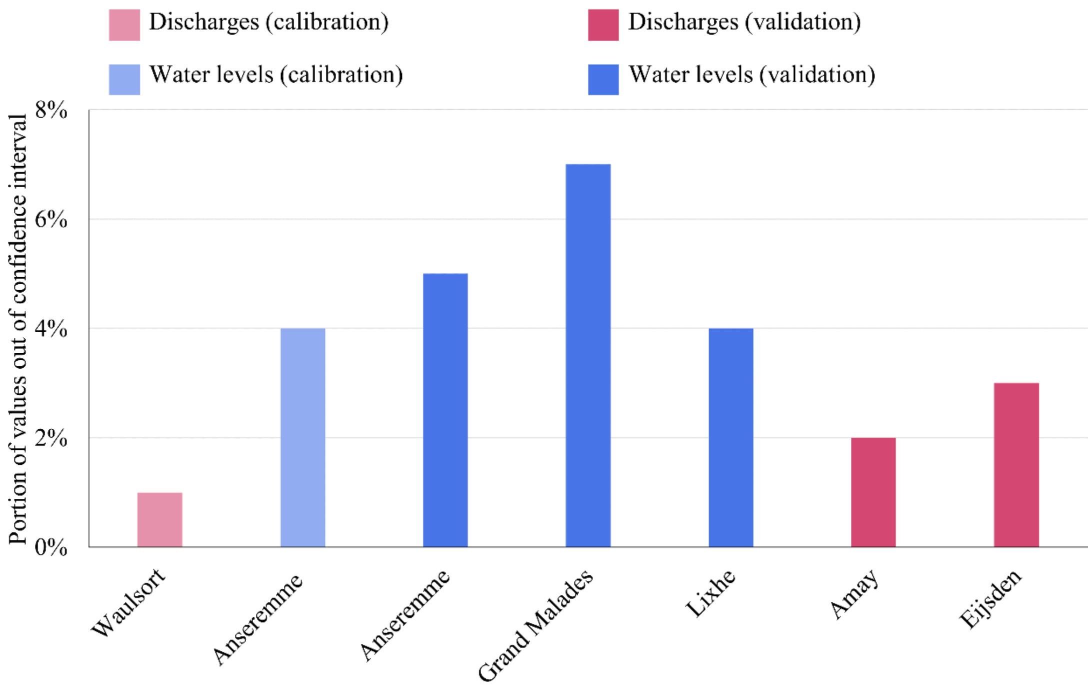

Discharges (calibration)
Discharges (validation)
Water levels (calibration)
Water levels (validation)
Portion of values out of confidence interval
8%
6%
4%
2%
0%
Waulsort
Anseremme
Anseremme
Grand Malades
Lixhe
Amay
Eijsden

Figure 17

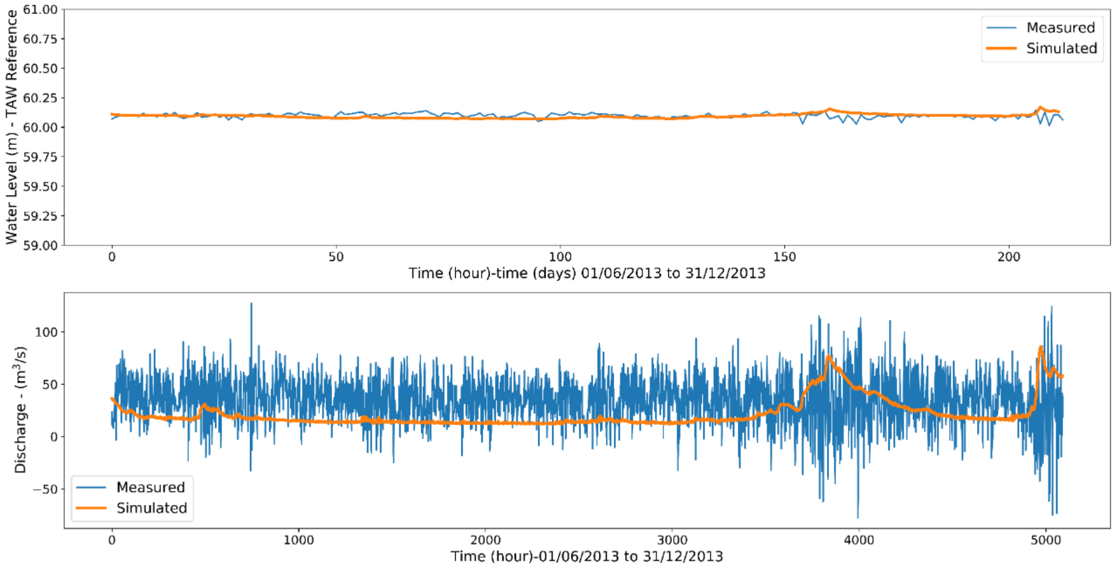
Water Level (m) - TAW Reference
61.00
60.75
60.50
60.25
60.00
59.75
59.50
59.25
59.00
Measured
Simulated
0
50
100
150
200
Time (hour)-time (days) 01/06/2013 to 31/12/2013
Discharge - (m^3/s)
100
50
0
−50
Measured
Simulated
0
1000
2000
3000
4000
5000
Time (hour)-01/06/2013 to 31/12/2013

Figure 18

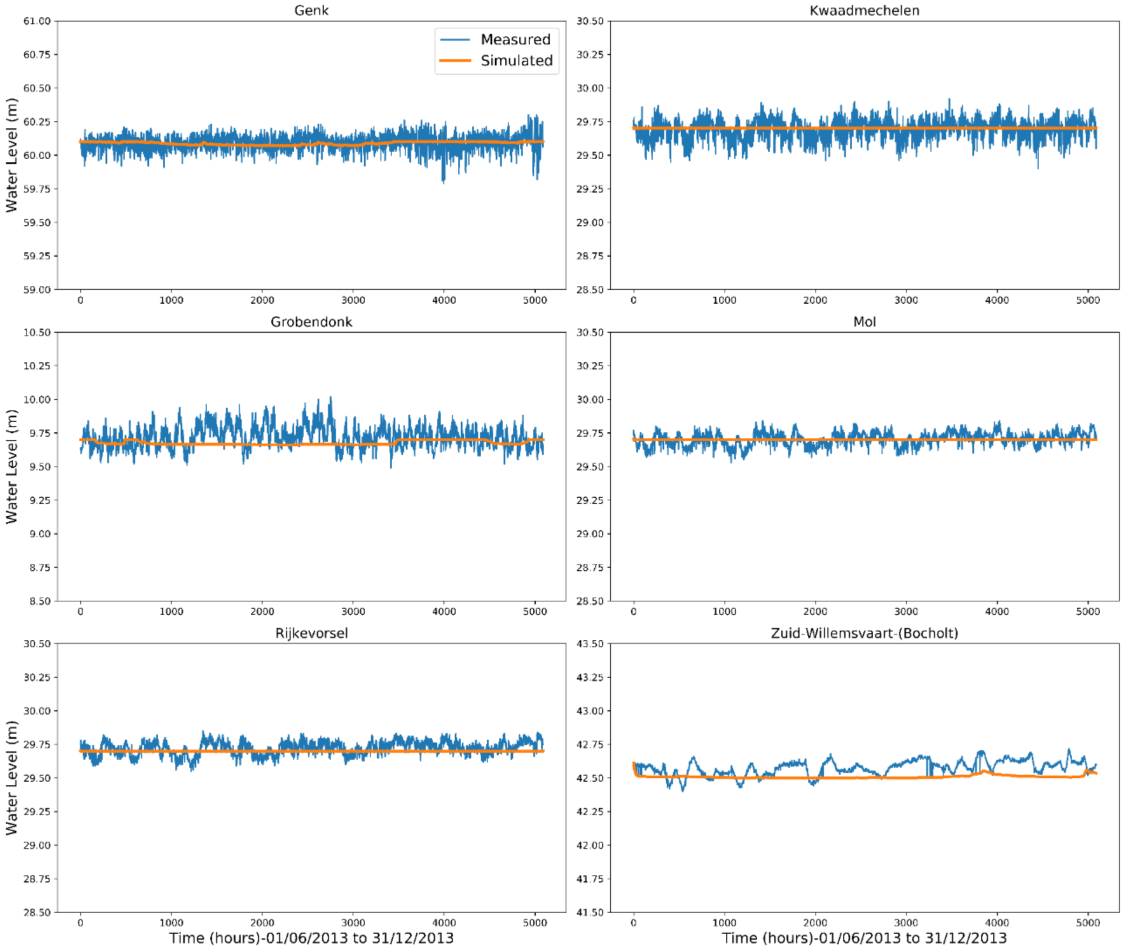
Genk
Kwaadmechelen
Grobendonk
Mol
Rijkevorsel
Zuid-Willemsvaart-(Bocholt)
Measured
Simulated
Water Level (m)
Time (hours)-01/06/2013 to 31/12/2013
0
1000
2000
3000
4000
5000
61.00
60.75
60.50
60.25
60.00
59.75
59.50
59.25
59.00
30.50
30.25
30.00
29.75
29.50
29.25
29.00
28.75
28.50
10.50
10.25
10.00
9.75
9.50
9.25
9.00
8.75
8.50
43.50
43.25
43.00
42.75
42.50
42.25
42.00
41.75
41.50

Figure 19

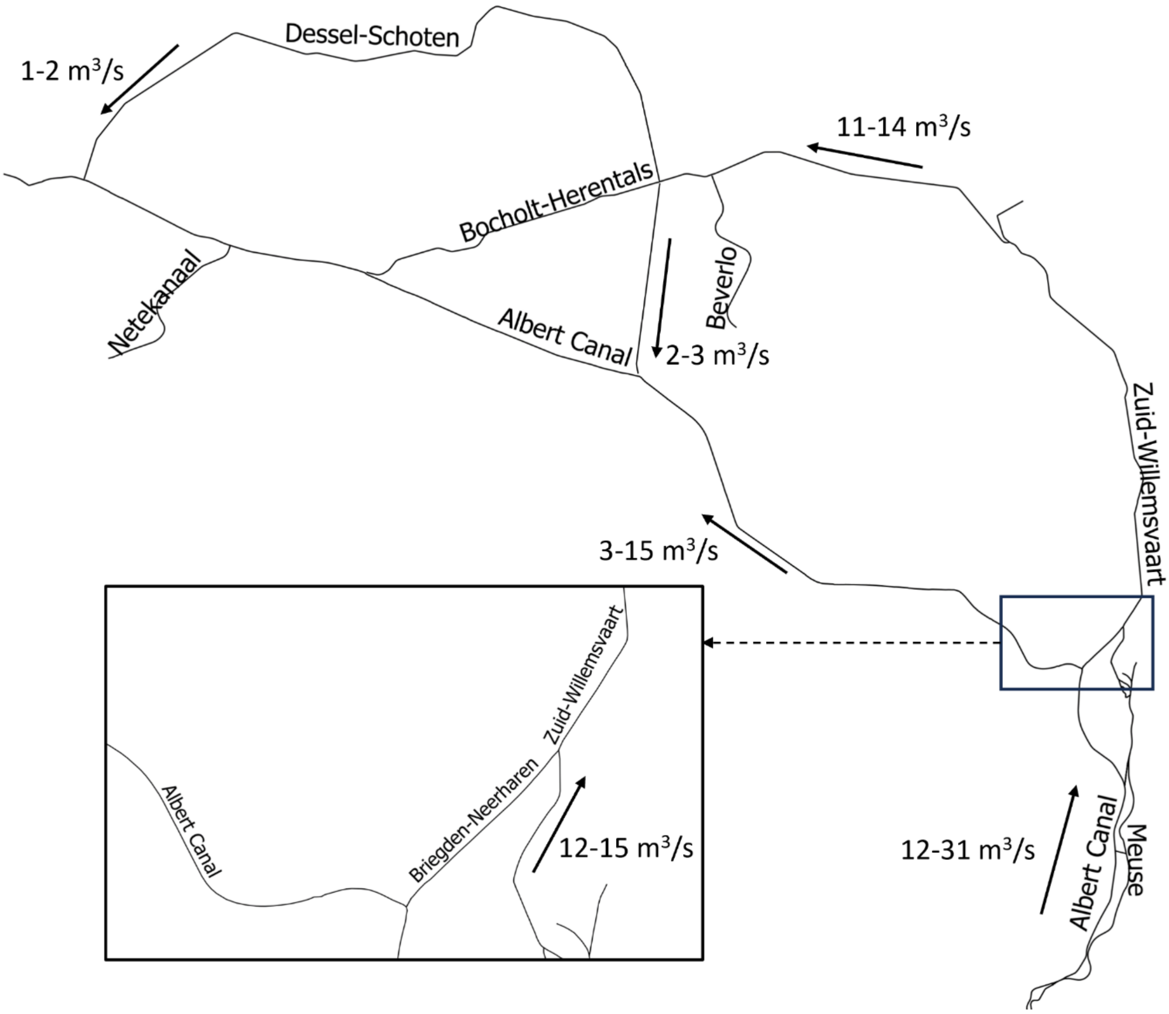
Dessel-Schoten
1-2 m³/s
11-14 m³/s
Bocholt-Herentals
Netekanaal
Beverlo
Albert Canal
2-3 m³/s
Zuid-Willemsvaart
3-15 m³/s
Zuid-Willemsvaart
Albert Canal
Briegden-Neerharen
12-15 m³/s
12-31 m³/s
Albert Canal
Meuse

Figure 20

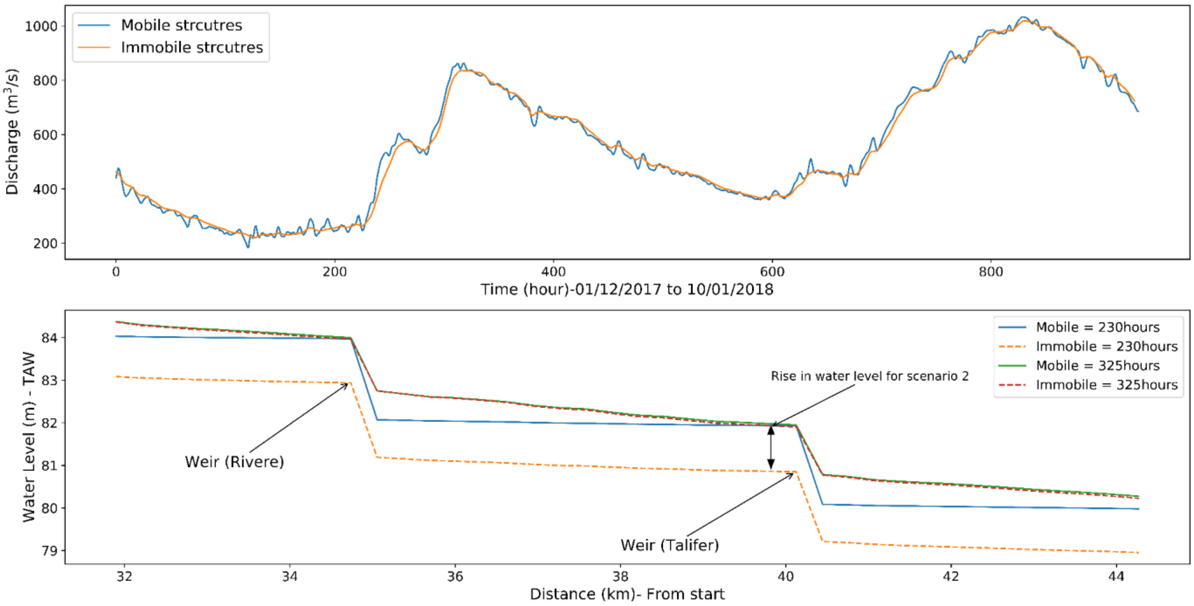
Mobile strcutres
Immobile strcutres
Discharge (m³/s)
Time (hour)-01/12/2017 to 10/01/2018
Mobile = 230hours
Immobile = 230hours
Mobile = 325hours
Immobile = 325hours
Rise in water level for scenario 2
Weir (Rivere)
Weir (Talifer)
Water Level (m) - TAW
Distance (km)- From start

Figure A1

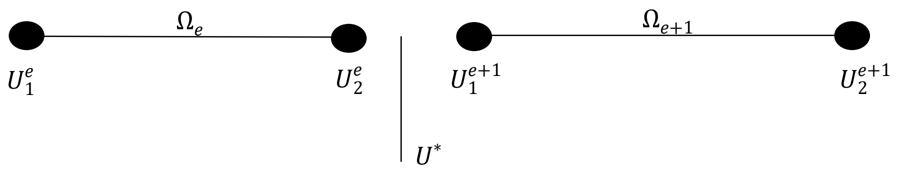

Figure A2

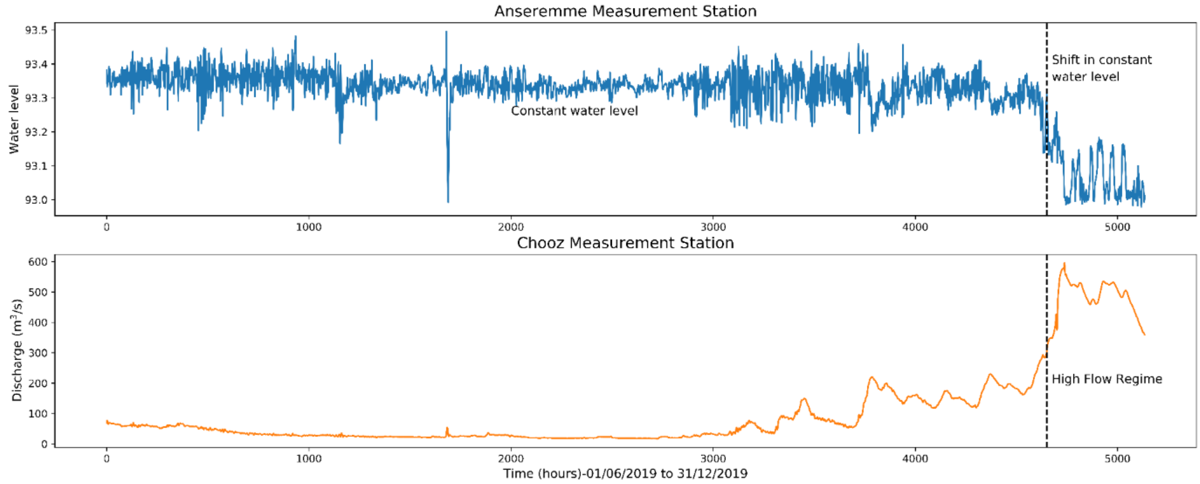
Anseremme Measurement Station
Water level
Constant water level
Shift in constant water level
Chooz Measurement Station
Discharge (m³/s)
High Flow Regime
Time (hours)-01/06/2019 to 31/12/2019

Figure A3

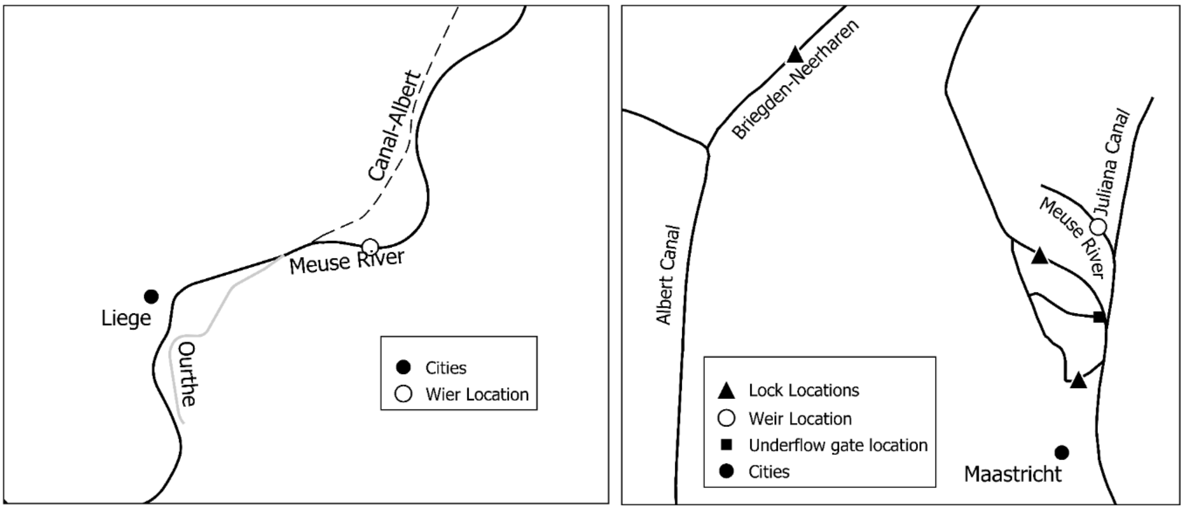
Canal-Albert
Meuse River
Liege
Ourthe
Cities
Wier Location
Briegden-Neerharen
Albert Canal
Juliana Canal
Meuse River
Lock Locations
Weir Location
Underflow gate location
Cities
Maastricht

Figure A4

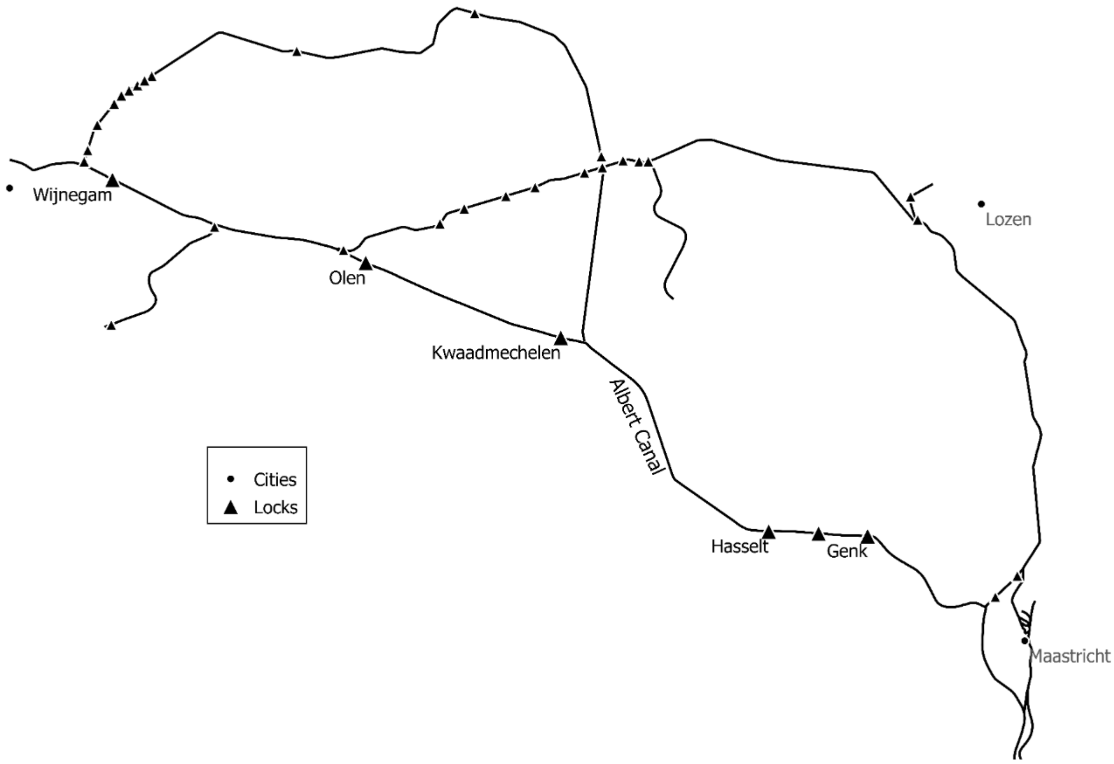

Wijnegam
Olen
Kwaadmechelen
Albert Canal
Lozen
Hasselt
Genk
Maastricht
Cities
Locks

Figure A5

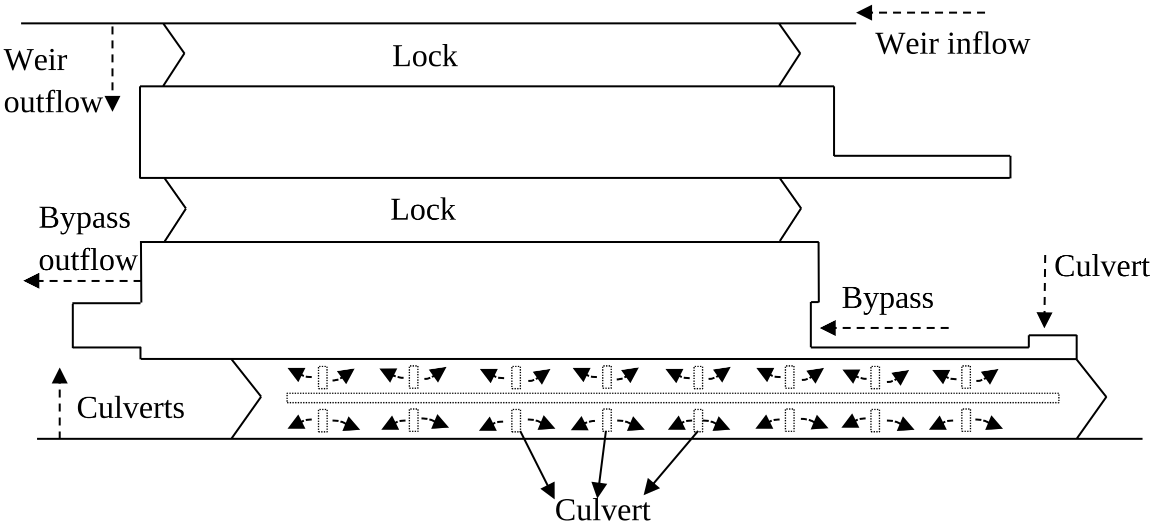
Weir inflow
Weir
outflow
Lock
Lock
Bypass
outflow
Culvert
Bypass
Culverts
Culvert

Figure A6

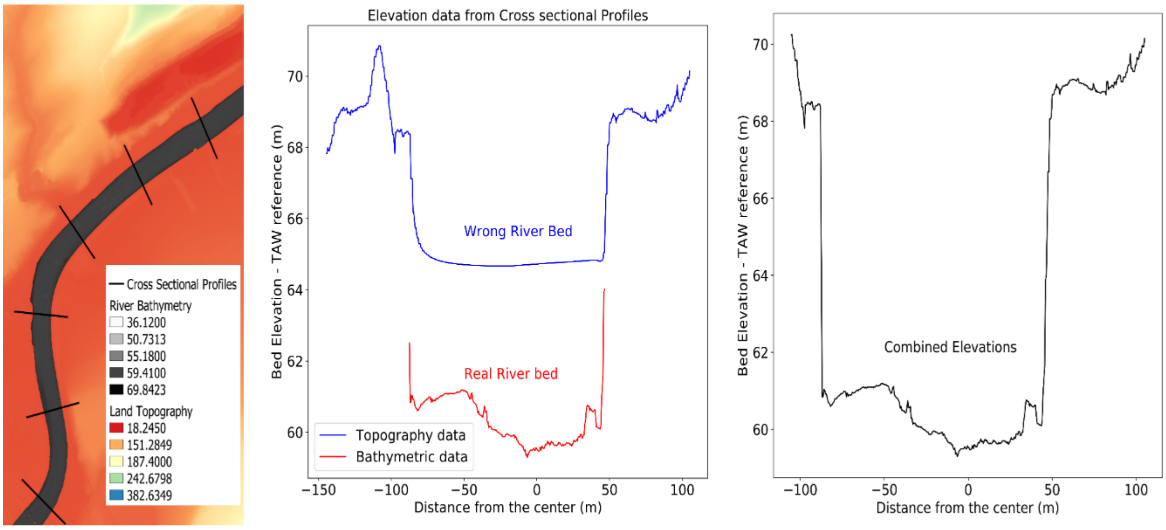
Cross Sectional Profiles
River Bathymetry
36.1200
50.7313
55.1800
59.4100
69.8423
Land Topography
18.2450
151.2849
187.4000
242.6798
382.6349
Elevation data from Cross sectional Profiles
Bed Elevation - TAW reference (m)
Distance from the center (m)
Wrong River Bed
Real River bed
Topography data
Bathymetric data
Combined Elevations
Bed Elevation - TAW reference (m)
Distance from the center (m)